water

MDPI

Supplementary material

The Effect of Organic Carbon Addition on the Community Structure and Kinetics of Microcystin-Degrading Bacterial Consortia

Derek Manheim *, Yuen-Ming Cheung and Sunny Jiang

Department of Civil and Environmental Engineering, University of California, Irvine, CA 92697, USA; mingc1728@gmail.com (Y.-M.C.); sjiang@uci.edu (S.J.)

* Correspondence: dmanheim@uci.edu; Tel.: +1-858-334-8757

Number of Figures: 19; Number of Tables: 11

(1) ELISA and UPLC-MS/MS Results

Figures S1 and S2 depict typical calibration curves used in both the ADDA-ELISA analysis and UPLC-MS/MS confirmations of microcystin (MC) concentration. Excellent agreement was observed between the standard concentrations and the response of either measurement technique for all replicate experiments (r^2 approaching 1). These results ensured that each measurement of MC concentration was reproducible and subject to low variability.

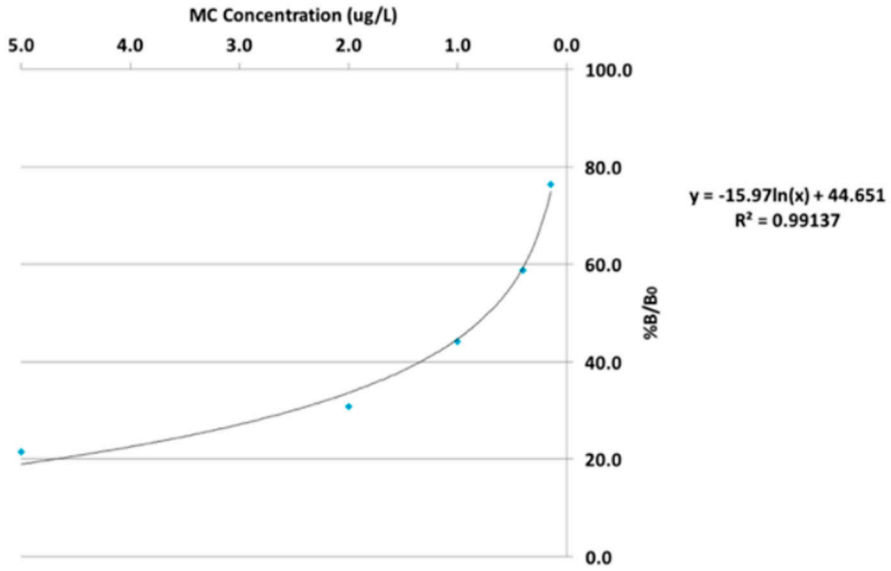

Figure S1 Sample calibration curve for ELISA tests for determination of MC concentration in batch degradation experiments. The correlation coefficient in this case was 0.99137, indicating good agreement between measured and standard concentrations.

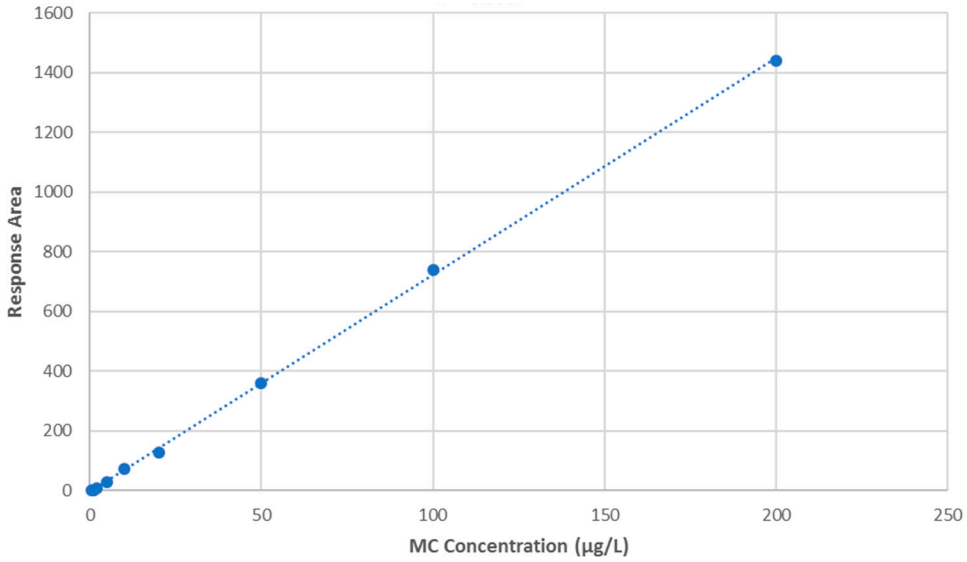

Figure S2 Sample calibration curve for UPLC-MS/MS tests for comparison against ELISA tests. The correlation coefficient in this was 0.9997, indicating very good agreement between measured and standard concentrations.

(2) Flow Cytometry Results

For consortia cultured without the presence of ethanol, optical density was not sensitive enough to detect changes in the concentration of MC-degrading bacterial cells. Therefore, flow cytometry was used to qualify the changes in cell counts during additional batch biodegradation experiments or each consortium in the presence of MC-LR. In brief, a Novocyte Flow cytometer (ABEA Biosciences) equipped with a single 488 nm excitation laser was used for bacterial cell detection. The cells were diluted, fixed, and stained with fluorescent SYBR Gold dye following a similar procedure presented by Huang et al. (2016) [1]. Based on the SYBR Gold fluorescent properties, the forward scatter (FSC-H), side scatter (SSC-H), and main fluorescence intensity (FITC-H) channels were monitored during measurement. Flow cytometer settings were set to the following for each run: slow flow rate, 35 µL of sample injection, and FSC-H/FITC-H cutoffs at 150 and 500. respectively. These cutoffs were empirically determined to properly separate the bacterial signal from the smaller virus or debris particle signal.

Figure S3 illustrates the results of the 11B consortia degrading MC-LR at an initial concentration of 100 µg/L after three replicate experiments. Other consortia (i.e., 10B and LSB) shared similar cell growth behavior of the 11B consortium (data not shown). MC-LR was rapidly degraded by 11B consortium 2-4 days after the initial inoculation. Cell growth was highly variable for this consortium after 27, 66, and 98 hours (1, 3, and 4 days) of the duration of the experiment. However, there was relatively low variability in measured MC concentrations throughout the course of the experiment, indicating that MC metabolism was similar across each replicate experiment. Differences in cell growth may be attributed to a wide range in factors, including the composition of the initial inoculum. Although the initial cell counts were relatively equivalent across replicates (as intended), it was difficult to control, for example, the ratio of the initial number of MC degrading organisms to non-degrading organisms, which may have substantially influenced the cell growth profiles. Overall, the flow cytometry data was useful as it indicated that cell growth was occurring in each consortium using MC as the sole carbon and energy source and that the initial bacterial cell concentrations were relatively uniform across each experimental replicate.

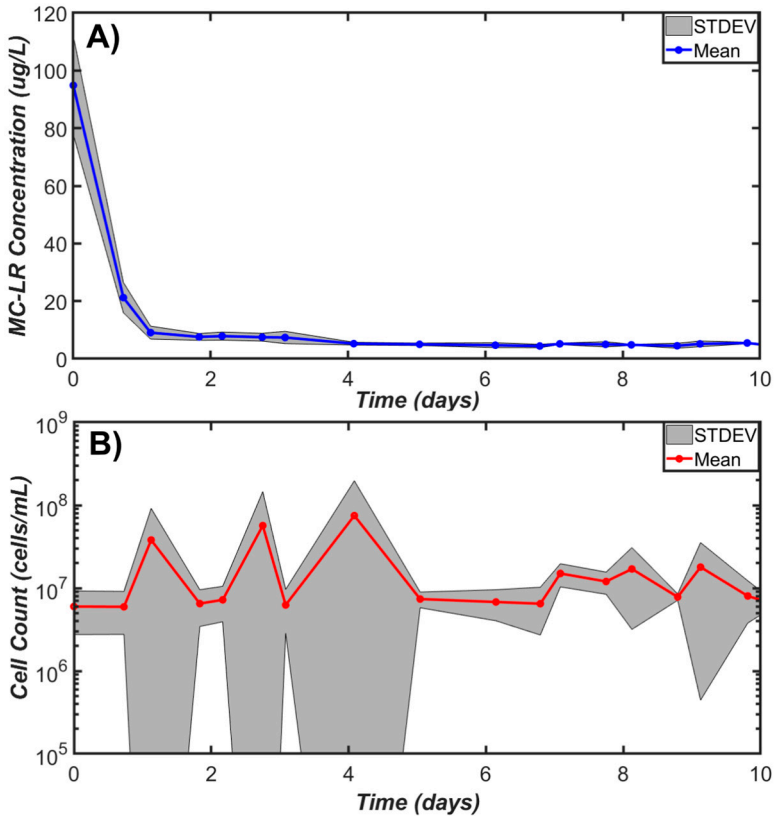

Figure S3 MC-LR batch biodegradation experiment for the 11B consortia cultured without ethanol. Both the A) concentration of MC-LR (blue) measured using ELISA and B) cell counts (red) measured by flow cytometry are reported. Solid lines indicate the mean of three individual replicates, whereas grey shading indicates one standard deviation of the replicated measurements. The y-axis for cell count concentration is plotted on a log (base 10)-scale.

(3) MC-LR Abiotic Degradation Experiments

Control experiments (MC-LR without added consortia or ethanol) were run in triplicate to assess the effect of abiotic degradation potentially taking place during the batch biodegradation experiments (Figure S4). Experimental conditions for these experiments were kept identical to those described for batch biodegradation; however, monitoring was only performed for 4-days (shaken, room temperature, same volume and sterile tissue flasks used, 200 μg/L MC-LR initial concentration). As observed in Figure S4, there was a slight decline in MC-LR during experimentation, with some variation observed across replicates. The decline in MC concentrations may be attributed to sorption to the tissue flask rather than abiotic degradation as the experiments were performed in the dark and under room temperature (ruling out photo or thermal degradation) and the stability of MC is very high compared to other chemicals or toxicants.

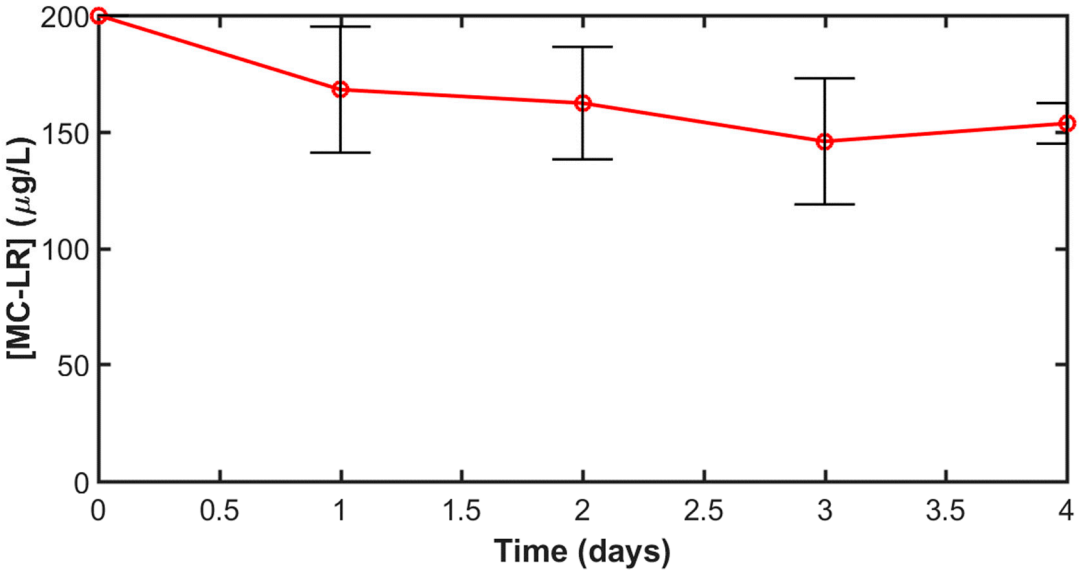

Figure S4. Concentration of MC-LR as observed during the batch control experiments.

(4) Derivation of the Bi-Phasic Kinetic Model

The derivation of the analytical solution for the bi-phasic kinetic model presented in Equation 1 is shown below and is similar to that presented by Ouiroga and co-workers [2].

$$\frac{dC}{dt} = -KCX \tag{1}$$

First, a substitution is made for the microorganism concentration (X) given that the substrate (MC concentration) is rate limiting by introducing the cell yield coefficient (Y), resulting in Equation 4.

$$Y = \frac{X - X_0}{C_0 - C} \tag{2}$$

$$X = Y(C_0 - C) + X_0 \tag{3}$$

$$\frac{dC}{dt} = -KYC^2 + C(KX_0 + KYC_0) \tag{4}$$

The proposed model also considers some fraction of the initial substrate (MC) to be non-biodegradable, which is realistic given that complete degradation of MC often is not performed by the degrader population (and depends on the non-degrader population present).

$$C_T = C_B + C_{NB} \;\; and \;\; C_{T0} = C_{B0} + C_{NB} \tag{5}$$

where C_T is the total substrate, C_B is the biodegradeable substrate, and C_{NB} is the non-biodegradable substrate portion, C_{T0} is the initial total susbtrate, C_{B0} is the initial biodegradeable substrate, in which the non-biodegradeable substrate remains non-transformed during degradation.

Substituting the above relations for total substrate and grouping together like terms, three rate coefficients are observed, K_0, K_1, and K_2. The mathematical meanings of each of these kinetic constants are described below (Equations 7-9).

$$\frac{dC}{dt} = K_2C^2 + K_1C + K_0 \tag{6}$$

$$K_2 = -KY \tag{7}$$

$$K_1 = KY\left(\frac{X_0}{Y} + (C_{T0} - C_{NB}) + 2C_{NB}\right) \quad (8)$$

$$K_0 = -KY\left(\frac{X_0}{Y}C_{NB} + (C_{T0} - C_{NB})C_{NB} + {C_{NB}}^2\right) \quad (9)$$

The physical meaning of each of these constants can be determined by factoring Equation 6 and defining a new set of model parameters, p, q, and h. It can be shown mathematically that h is one limiting solution of the quadratic equation, and represents one solution where biodegradation rates are at a minimum (dc/dt = 0). In this way, h is termed the maximum amount of substrate available for biodegradation. On the other hand, q is another limiting case from the quadratic equation where biodegradation rates reach a minimum. Thus, q signifies the non-biodegradable fraction of substrate remaining when the biodegradable substrate is exhausted. Finally, when substituting K_1, K_2, and K_0 into Equation 10, it is evident that the p value represents the maximum specific growth rate of the microorganisms ($\frac{1}{X}\frac{dX}{dt}$).

$$p = \sqrt{(K_1^2 - 4K_2K_0)} \quad (10)$$

$$q = \frac{-K_1 + p}{2K_2} \quad (11)$$

$$h = \frac{-K_1 - p}{2K_2} \quad (12)$$

where h represents the maximum amount of substrate (MC-LR) available for biodegradation (μg/L), q represents the non-biodegradable portion of MC-LR (μg/L), and p represents the maximum growth rate of the microorganisms (1/day).

(5) Summary of Model-Data Fitting Procedure and Metrics

DREAMzs (v1.0), a variant of the well-known Bayesian, Differential Evolution Adaptive Metropolis (*DREAM*) algorithm, was used to estimate the posterior distribution of model parameters and associated half-lives. *DREAMzs* differs from *DREAM* in that it samples from the past states of each designated Markov chain exploring the specified parameter space and was selected for this study for the following advantages: a) a smaller number of chains is required to search the parameter space (reducing CPU time); b) the CPU time can be further reduced since each chain can run on a different processor (better parallel distribution); and c) outlier chains do not need as forceful of treatment as compared to *DREAM* [3]. Advantage c) was particularly important since the parameter space for this kinetic model was marked by a very large number of local minima.

The specific settings used to run the *DREAMzs* algorithm are described in Table S1. The choice of objective function was set to Gaussian likelihood without measurement error (with the assumption that the error residuals are normal, independent, and homoscedastic), as the sample size (n=3) was small. With a smaller number of replicates, the standard deviation will vary considerably by chance; therefore, weighting by the measurement error should, in most cases, always be avoided [4].

Table S1 – DREAM_ZS settings for Model-Data Fitting Procedure.

Parameter Setting	Nominal Value
Objective Function	Gaussian Likelihood: measurement error integrated out
Number of Markov Chains (*N*)	6
Number of Generations (*T*)	50,000
Prior Distribution	Uniform
Boundary Handling	Reflection
Number of Crossover Values (*nCR*)	3

Number of Chain Pairs for Proposal (δ)	3
Random Error for Ergodicity (λ)	0.05
Randomization (ζ)	0.05
Probability of Jump Rate	1
Adapt Selection Probability Crossover	Yes
Scaling Factor of Jump Rate (*b0*)	0.75

For all cases, a small number of chains (~6-15) and a high number of generations (50K-200K) resulted in convergence of the search algorithm for all datasets (Figure S5). The number of chains for low-dimensional problems (d<10) in *DREAMZS* was recommended to at least 3; therefore, between 6-15 were used to be as conservative as possible. For runs requiring greater than 6 chains to reach convergence, outlying chains (with poor progress to the global minimum solution) were removed so that the number of chains compared was always consistent between experiments (6). In addition, the number of posterior samples (n) used after each fitting procedure was set to 25,000 (discarding half of samples for "burn in"). If the number of generations required to reach convergence was greater than 50,000, the last 25,000 samples were used to keep the number of posterior samples consistent between experiments. Convergence of the search algorithm to the target distribution was observed when the multivariate R_{hat} statistic, which compares the variance of the parameter distributions both within and between chains, reached a value below the threshold value of 1.2 [3,5] (Figure S5).

The prior distribution was set to a uniform range between 195-205, 0-10, and 0-10 for the three parameters h, q, and p due to lack of information provided in the literature concerning the typical range in these parameters. The scaling factor jump rate (*b0*) was another parameter that was changed from the default value, where it was reduced from 1 to 0.75 to allow improved mixing and acceptance probabilities for each chain [3]. The remaining settings used in *DREAMZS* were all default values, as pre-specified by the algorithm.

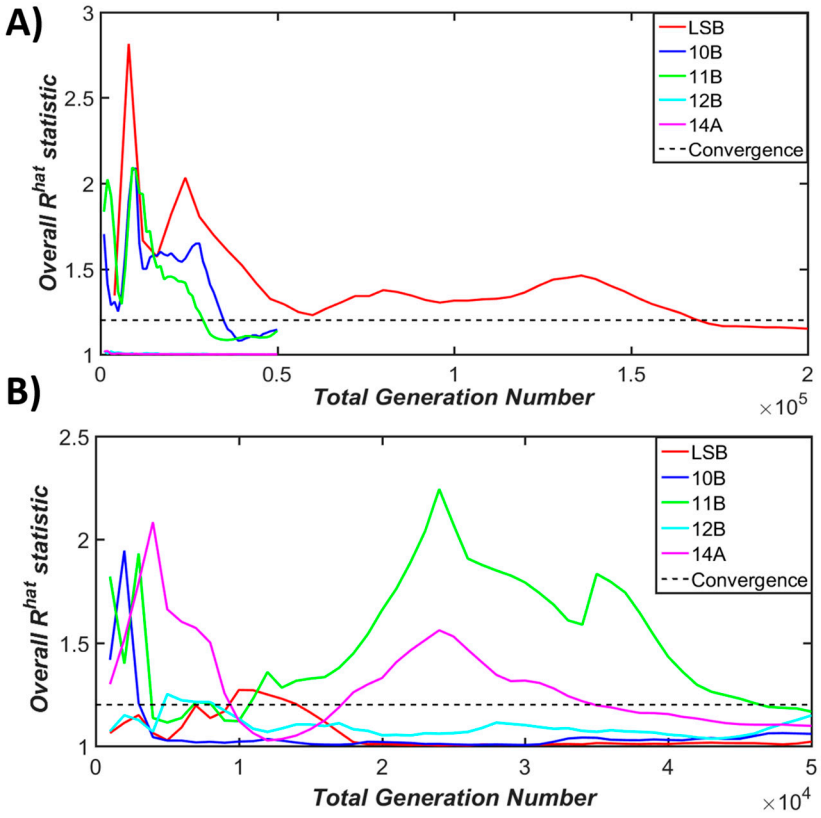

Figure S5 Evolution of the multivariate convergence statistic (Rhat) using the DREAM_ZS algorithm for a) consortia without and b) consortia with the presence of ethanol.

A summary of the best performing parameter sets (maximum log-likelihood) and the mean/95% credible intervals for the parameter estimations is presented in Tables S2 and S3. In addition, the marginal densities of the posterior parameter distributions are plotted in Figure S6. To reiterate the meaning of each model parameter, *h* represents the maximum amount of substrate (MC-LR) available for biodegradation (μg/L), *q* represents the non-biodegradable portion of MC-LR (μg/L), and *p* represents the maximum growth rate of the microorganisms (1/day). The credible intervals were generally widest (highest uncertainty) for the non-biodegradable fraction of MC (*q*), especially for 10B, 12B, and LSB without the presence of ethanol (Table S3). These results can be observed visually (Figure S6) as the spread of the distribution for some model-data fits for q appears uniform across the specified interval of the prior parameter distributions. This wide interval suggests that there was an array of potential local minimum solutions in the parameters search space, and possibly some correlation between parameters. The posterior distributions for the maximum specific growth rates (*p*) and the initial concentration of biodegradable substrate (*h*) were well defined for all model-data fitting procedures (with best performing parameters close to the peak of all distributions), with reasonable credible intervals observed (Table S3). The shape of the posterior parameter distributions for p appeared gaussian for most consortia, with and without ethanol, while the shape of the parameter distributions for h were negatively skewed, with many parameter values congregating close to the initial concentration of 200 μg/L. The posterior distribution of half-lives for MC biodegradation were well defined for most cases; however, some discontinuities in the distributions were observed for both the 11B with ethanol and LSB without ethanol cases (Figure S6).

Table S2 – Best Performing Parameter Sets and Associated Fitting Metrics.

Consortia ID	h (μg/L)	q (μg/L)	p (1/day)	$t^{1/2}$ (days)	r^2	RMSE
LR-NE-10B	200.0003	1.82	6.80	1.98	1.00	0.4299
LR-NE-11B	200.0001	1.63	6.69	2.12	1.00	0.4526
LR-NE-12B	204.9624	0.098	1.27	2.94	0.745	39.10
LR-NE-14A	204.9597	0.419	1.36	2.75	0.672	44.99
LR-NE-LSB	200.0001	1.69	6.81	2.15	1.00	0.3141
LR-WE-10B	200.0004	1.44	3.87	3.38	0.975	14.52
LR-WE-11B	200.0000	2.43	8.05	2.27	1.00	0.1451
LR-WE-12B	200.0000	0.169	4.58	3.43	0.995	6.943
LR-WE-14A	200.0000	1.97	9.87	2.45	1.00	0.2539
LR-WE-LSB	200.0016	0.710	2.64	4.43	0.975	12.63

Table S3 – Summary of Posterior Parameter Distributions.

Consortia ID	h (μg/L)		q (μg/L)		p (1/day)		$t^{1/2}$ (days)	
	μ	95% C.I.	μ	95% C.I.	μ	95%C.I.	μ	95%C.I.
LR-NE-10B	200.0025	[200.0003,200.0121]	1.78	[1.08,2.43]	5.97	[4.93,6.78]	1.976	[1.967,1.981]
LR-NE-11B	200.001	[200.0002,200.0052]	1.57	[0.604,2.43]	6.03	[4.88,6.65]	2.14	[2.12,2.18]
LR-NE-12B	202.4767	[199.9905,204.8917]	4.99	[0.238,9.74]	1.99	[1.05,6.28]	2.74	[0.733,4.01]
LR-NE-14A	202.3028	[197.6178,204.8869]	5.10	[0.252,9.76]	2.71	[1.14,8.13]	2.14	[0.56,3.67]
LR-NE-LSB	200.0004	[200.0000,200.0012]	1.61	[0.912,2.26]	6.47	[5.53,7.40]	2.16	[2.14,2.19]
LR-WE-10B	201.353	[200.0012,204.706]	4.71	[0.219,9.69]	1.92	[1.08,3.59]	3.28	[2.55,3.96]
LR-WE-11B	200.0000	[200.0000,200.0000]	2.34	[1.88,2.69]	7.59	[6.96,8.07]	2.30	[2.27,2.35]
LR-WE-12B	201.0049	[200.0000,204.594]	4.64	[0.199,9.67]	2.22	[1.07,4.58]	3.37	[2.68,4.00]
LR-WE-14A	200.0184	[200.0000,200.0042]	1.95	[0.135,6.43]	7.48	[4.36,9.72]	2.47	[2.38,2.56]
LR-WE-LSB	201.269	[200.0020,204.643]	4.72	[0.204,9.72]	1.41	[0.806,2.64]	4.41	[3.82,5.12]

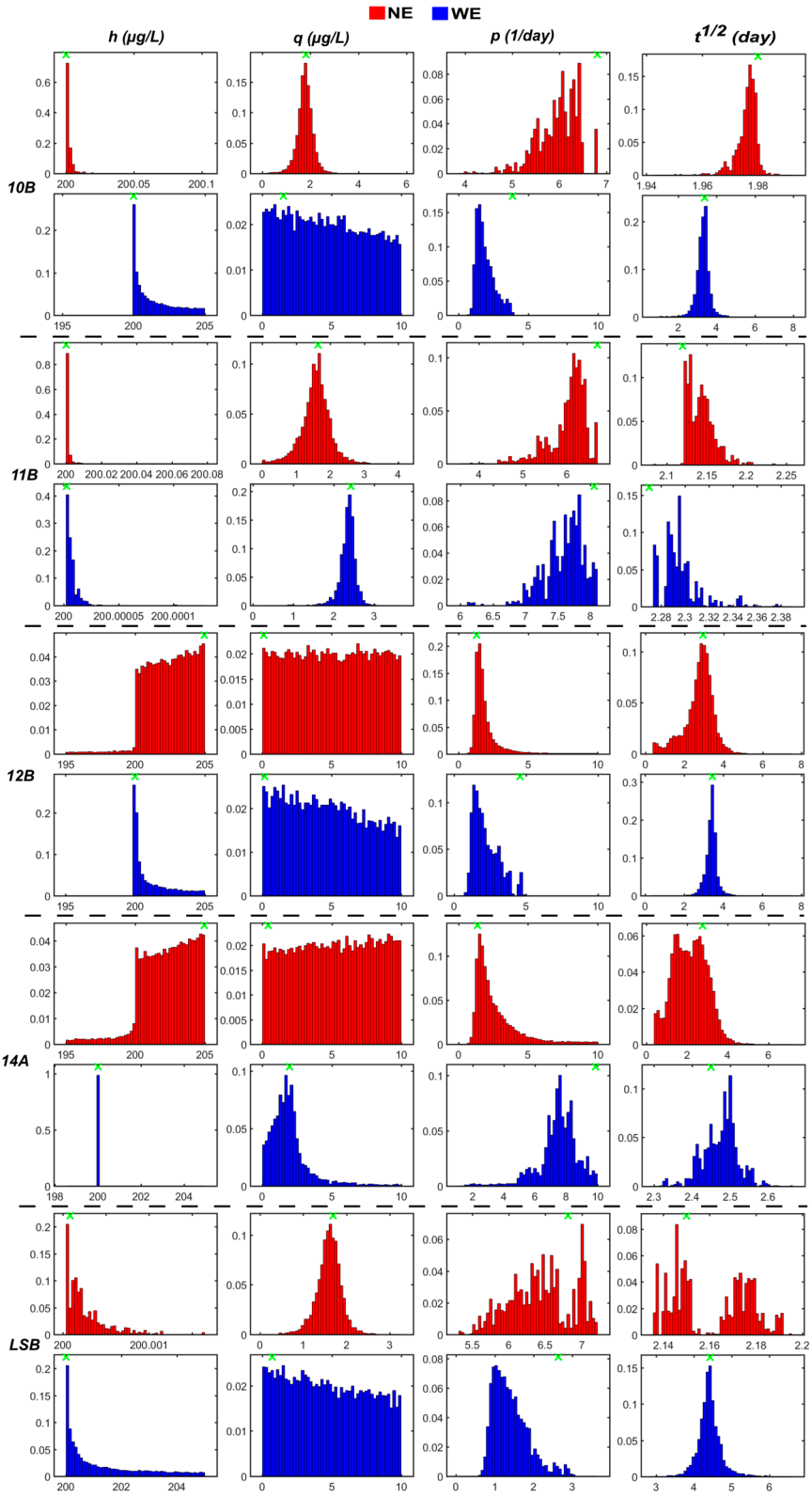

Figure S6 Marginal densities of parameters and half-lives developed from DREAM_ZS for each consortium without (red) and with (blue) the presence of ethanol. Green crosses (on the top of each plot) indicate the best performing parameters (and half-lives) associated with each distribution.

A potential reason for the lack of definition of the posterior distribution of some parameters (most often the non-biodegradable fraction of MC, *q*) may be due to either structural issues of the model (structural identifiability) or the quality of the data collected (practical identifiability) [5]. Since

the model structure used was relatively simplistic and previous studies have determined that the Monod kinetic model is globally identifiable, we can assume that the main problem is not due to structural identifiability, but rather parameter estimability [7]. In the case of estimability, we are concerned with whether we can estimate unique values of each parameter given the quality of the experimental data collected [6]. For many empirical models, such as the well-known Monod kinetic model, the initial conditions of the experiment (i.e., the initial biomass or substrate concentrations) have a drastic effect on whether unique parameters can be estimated [7–10]. In addition, a parameter may not be estimable if a) the model predictions are not sensitive to the parameter value or b) the effect of the parameter on model predictions is correlated with the effects of other parameters, where the latter is generally the case for unstructured bacterial growth models [6,9].

Thus, the degree of linear correlation between parameter values was evaluated using Pearson's correlation coefficients to assess whether parameter correlation was the main issue affecting estimability. This analysis indicated that there was a strong, significant negative correlation between the parameters h and p for all consortia, with and without ethanol (Table S4). For most cases, there was also a slight positive correlation between the parameters q and p, and a slight negative correlation between parameters h and q for all consortia, with and without ethanol (Table S4). These results indicate that, due to some inherent correlations between parameter values, the parameter estimability was low for some experimental data. The presence of these correlations provides evidence as to why in some cases the distribution of the non-biodegradable fraction of microcystin, q, was ill-defined.

Table S4 – Summary of Pearson's correlation and p-values for different model parameters.

Consortia I.D.	h vs. q		h vs. p		q vs. p	
	rho	p-value	rho	p-value	rho	p-value
10B-NE	-0.1510	0	-0.6810	0	0.1726	0
10B-WE	0.0174	1.54E-11	-0.6776	0	9.85E-04	0.7026
11B-NE	-0.1649	0	-0.6198	0	0.2690	0
11B-WE	-0.3956	0	-0.7708	0	0.3797	0
12B-NE	-0.0146	1.55E-08	-0.4813	0	0.0457	3.70E-70
12B-WE	0.0646	3.15E-138	-0.6766	0	-0.1002	0
14A-NE	-0.0389	3.06E-51	-0.5214	0	0.0533	1.17E-94
14A-WE	0.1515	0	-0.3655	0	-0.2825	0
LSB-NE	-0.3259	0	-0.8949	0	0.3398	0
LSB-WE	0.01	1.02E-04	-0.7529	0	-0.0118	4.78E-06

(6) Monte Carlo Simulations for Comparison of Alpha Diversity Metrics

Monte Carlo (MC) simulations were carried out to arrive at statistical distributions in true Alpha diversity metrics. The first step of this process was to develop an empirical relationship between mean relative abundance and the standard deviation expected among experimental replicates for corresponding taxa within a given community. By "experimental" replicates we refer to the combination of biological and technical replicate classes. Biological replicates can be defined as sampling multiple times at a given location and then performing identical 16S rRNA processing on the replicated samples [11,12]. The 16S rRNA processing protocol includes everything from sample preparation and DNA extraction, to pyrosequencing and downstream analysis (i.e., QIIME). Biological replication includes uncertainty related to the heterogeneity of the bacterial populations at the location of sampling as well as uncertainty related to the measurement/processing techniques. Technical replicates, however, are defined as processing a single sample from a location or treatment multiple times to solely assess the uncertainty in the measurement/processing technique [11,12]. We focused our search to obtain relevant data from studies analyzing bacterial community structure, as opposed to other microbes (from environmental samples only). Both mean relative abundances and

standard deviations of relative abundances were compiled from these studies (from at least 2 technical replicates) to develop the empirical model described above (Table S5).

A total of 10 metagenomic studies [13-22] were ultimately used to develop the empirical relationship between taxon mean relative abundance and expected standard deviation among replicates (Table S1). The pooled data from all these studies provided a sufficient number of samples to develop the empirical model (N = 1,188). Ideally, studies that performed biological replicates were more desirable, as they included uncertainty corresponding to both the community composition at the sampling location and the potential measurement error. However, very few studies that conducted biological replicates were found in the literature that presented relative abundance data on the genus level of analysis. In this way, we supplemented studies that performed biological replicates (5) with those that only performed technical replicates to aid in the development of this empirical model (5).

As observed in Table S5, the studies selected sampled a diverse array of environmental media for conducting the bacterial community analyses, ranging from drinking water, wastewater, seawater, soil, and aquifer sediments. The studies selected were split evenly between sequencing platforms, where half used the 454-pyrosequencing technology (as in this study) and the other half relied on Illumina MiSeq technologies. A majority of studies targeted the V4 region of the 16S rRNA, which was close to the region targeted in this study. In addition, most of the studies incorporated the QIIME/Greengenes analysis pipeline and reference database, which was nearly identical to that selected in this study (Table S5).

Table S5 – Summary of studies selected to develop the empirical model.

Reference	Source Location	Environ. Media	Seq. Platform	16S Region	Analysis Pipeline /Ref Database	Tax. Level	# Replicates	Type of Replicate
[13]	North Shore Channel, Chicago, USA	Stormwater/ Wastewater	Illumina MiSeq	V1-V3	QIIME/ Greengenes	Genus	2	Biological
[14]	Laboratory cultures, isolated from Mediterranean Sea	Seawater	454-FLX Titanium	V2-V3	QIIME/ Greengenes	Genus	3	Technical
[15]	Farm in Portugal	Soil	454-FLX Titanium	V3-V4	QIIME/ Greengenes	Genus	3	Biological
[16]	Energy Farm, University of Illinois, USA	Soil	454-FLX Titanium	V4-V5	RDP Pipeline	Genus	4	Biological
[17]	Helmholtz Centre for Infection Research, Germany	Drinking Water	Illumina MiSeq	V3-V4	SILVA Pipeline	Genus	3	Technical
[18]	Tar oil contaminated aquifer, Germany	Aquifer Sediments	454-FLX Titanium	Unknown	GS Run Processor/Greengenes	Genus	3	Biological
[19]	Orchard near Beijing, China	Soil	Illumina MiSeq	V4	QIIME/Greengenes	Genus	3	Technical

[20]	Forest floor samples, Upper Michigan, USA	Soil	PacBio RS II	Unknown	MOTHUR Pipeline	Order	4	Biological
[21]	Laboratory grown cultures	Soil	Illumina MiSeq	V4	QIIME/Greengenes	Genus	3	Technical
[22]	Experimental Station, Harbin, China	Soil	Illumina MiSeq	V3-V4	QIIME/Greengenes	Genus	3	Technical

A non-linear, yet monotonic, relationship between taxon mean relative abundance and standard deviation of replicate measurements was observed from the compiled data. This monotonic relationship makes sense intuitively, as the abundance of a given taxon increases, the associated variability across replicate samples should also increase. The dependency structure between the mean relative abundance and standard deviation was deemed significant as the magnitude of Spearman's rho was high (0.84). To be as objective as possible, a non-parametric regression model (LOESS) was used to describe the compiled data. LOESS stands for locally weighted polynomial regression and is a simple, but powerful tool to model unknown, empirical relationships between variables [23]. LOESS provides a smooth interpretation of the relationship between two variables through use of two main model parameters, the polynomial order (λ) and the spanning parameter (α). In general, the polynomial order dictates what shapes the curve can take, while the spanning parameter balances "overfitting" vs. "smoothing" of the data [23]. Larger values of α (close to 1) will provide a smoother curve at the cost of a poorer fit, while smaller values of α (close to 0) provide an optimal fit, but a very haphazard (and non-generalizable) curve. In this study, we selected a polynomial of order two ($\lambda = 2$) and an optimal spanning parameter of 0.85 based on the procedure outlined in [23]. A bootstrap re-sampling approach (using N = 10,000 samples) was used to estimate both the 95% confidence and prediction intervals for the LOESS regression model. The algorithm presented by [24] was implemented in this study to develop the 95% confidence and prediction intervals of the empirical model.

Figure S7 portrays the results of the LOESS nonparametric regression and bootstrapping analysis. Given that the main underlying trend in the observed data is captured by the LOESS prediction, the regression model was concluded to satisfactorily predict the nonlinear relationship between mean relative abundance and standard deviation among experimental replicates. As observed in Figure S7, several data points fall outside the 95% prediction and confidence intervals and may be considered outliers in this analysis. In addition, most of the data points are clustered towards the origin of Figure S7 (where corresponding certainty in the regression is higher). This result was expected given that, on the genus level of analysis, most of the identified taxa among studies had low relative abundances (<10%). The uncertainty in the model predictions rises substantially when the mean relative abundance increases to 30% and beyond (Figure S7). This result was a direct consequence of the small number of data points compiled from the literature that were above a mean relative abundance of 30%. Since this was a locally weighted regression analysis, higher confidence would be achieved if the density of points above this mean relative abundance threshold of 30% was greater.

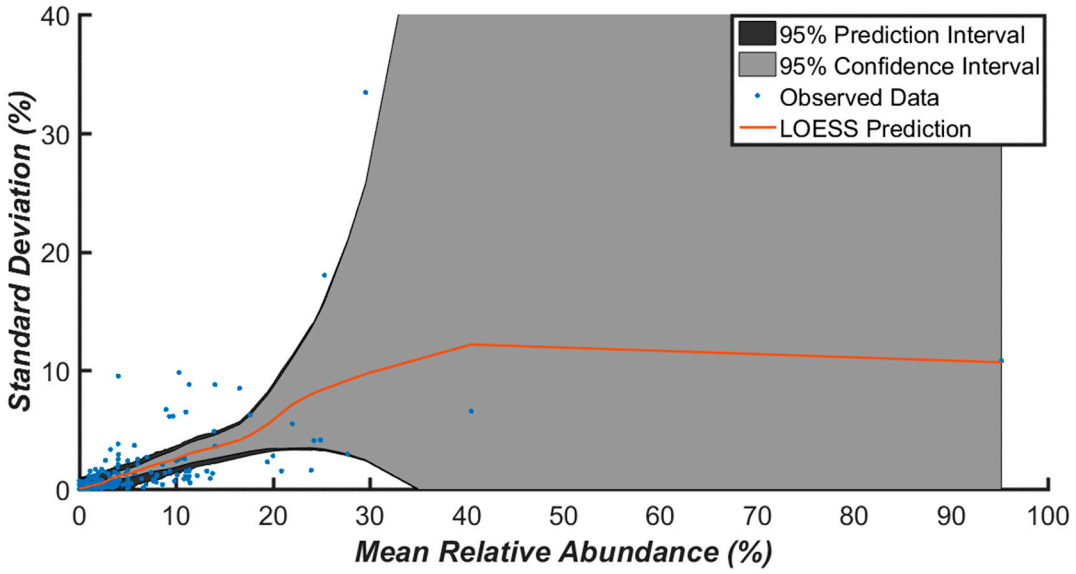

Figure S7 Empirical relationship developed between mean relative abundance and expected standard deviation among experimental replicates using the LOESS regression approach. Dark and light grey shading indicate the 95% bootstrapped prediction and confidence intervals for the LOESS predictions. The blue dots and red line correspond to the observed data points and best fitting prediction of the LOESS regression.

With the main empirical relationship between taxon mean relative abundance and expected standard deviation established, the main approach behind the MC simulations to determine distributions in true Alpha diversity metrics will now be described. The objective of the MC simulations was to randomly and repeatedly generate a new bacterial community composition, given the known extrapolated uncertainty in the experimental measurements, and calculate Alpha diversity metrics for each of these re-sampled communities. Figure S8 describes the main workflow of the MC simulations from start to finish. First, the experimental data containing the identified genus (rows) vs. absolute abundances (columns) for a given community is loaded and transformed into relative abundances (on a scale from 0-1).

After entering the main Monte Carlo loop (which is performed for N_{max} = 20,000 times), the following two steps (2, 3) involve sampling the relative taxonomic abundances for all genera within the community (Figure S8). We first assume that the measurement error (which includes uncertainty about the heterogeneity of each community within each location and the measurement methodology) is normally distributed. In addition, we center each normal distribution describing the uncertainty in taxonomic abundance from each location around the observed relative abundances obtained from the experimental results. Thus, given the mean relative abundance from step 1, step 2 involves randomly sampling the 95% prediction intervals of the LOESS regression to obtain the expected standard deviation across replicates. The 95% prediction intervals were approximated by a kernel density estimation (KDE) since the distribution of the predictions within each interval appeared to be non-parametric and multi-modal (data not shown). Using the obtained standard deviation, step 3 involves randomly sampling a relative abundance value from this normal distribution. Steps 2 and 3 are repeated until relative abundances have been sampled for all existing genera within the original community.

As the sampled standard deviations can vary, there is a possibility of selecting either a negative standard deviation or a negative relative abundance. To circumnavigate this issue, we only sample positive standard deviations from the empirical model. However, it is important to note the significance of a negative relative abundance draw. Instead of only sampling positive values (the right side of the normal distribution) for relative abundance, we assume that a negative relative

abundance is indicative of several replicates (out of how many were conducted) that may have demonstrated relative abundance values of 0. Thus, when a negative relative abundance value is obtained, we assume that this draw was effectively 0 (and not a member of the simulated community). Importantly, this step allows the MC simulations the probability of not drawing relative abundances for genera that were in fact experimentally observed, providing some measure of variability for richness-based measures of Alpha diversity for each community (true Alpha diversity measures of order 0).

The final two steps within the MC loop involve the re-sampling (4) and calculation of true Alpha diversity metrics (5) (Figure S8). With the relative abundances of the simulated community now sampled, a weighted re-sampling of the original community is performed to obtain absolute abundances for each genus (using a weighted random sample with replacement). Step (4) is essentially the main bootstrapping component of this procedure. Finally, the true Alpha diversity metrics are calculated using the absolute abundances sampled during the previous weighted bootstrapping step. This series of sampling and calculations is effectively repeated (N_{max} = 20,000 times) and a final distribution in true diversity metrics is obtained (Figures S9 and S10, Tables S6 and S7).

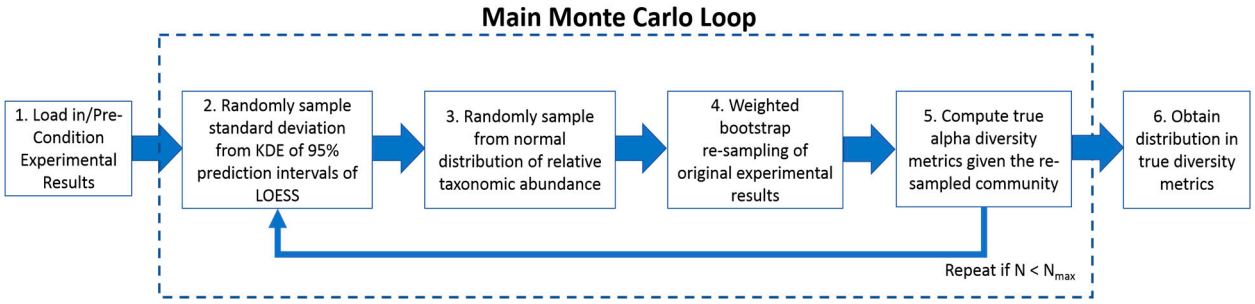

Figure S8 The MC algorithm developed to simulate distributions in true Alpha diversity metrics.

Typically, in many MC applications, N = 10,000 MC samples are enough to arrive at a parametric and stable distribution [25]. In this study, we found that 20,000 samples were necessary to arrive at a series of stable distributions for each true diversity order, all of which qualitatively appeared distinctly normal (Figures S9 and S10, Tables S6 and S7). The lack of extreme outliers (low kurtosis values) and characteristic bell shape of the plotted histograms indicated satisfactory fits to a normal distribution for most diversity orders describing each MC-degrading community. It is important to note that for some higher order diversity indices (q = 1-3) describing communities with the addition of ethanol, the resulting distributions were slightly right skewed, more notably for 10B and 12B consortia. This skew was confirmed with the relatively higher coefficient of variations observed for 10B (with ethanol) for the higher order diversity metrics (1-3) (Table S7). Otherwise, variability in simulated metrics generally increased moving from the far-right side of both Tables S6 and S7 (q =3) to the far-left side (q = -1), as the magnitude of the indices increased. Both the 10B and 12B communities (in the presence of ethanol), contained genera that had higher relative abundances (>30%) than the other MC-degrading communities analyzed. As the empirical model demonstrated higher uncertainty in predicting the standard deviations in replicated measurements for high relative abundances (>30%), deviation from a perfectly normal distribution was as expected. However, other, more complex parametric distributions were not applied in this study to account for the skew in these aforementioned probability distributions.

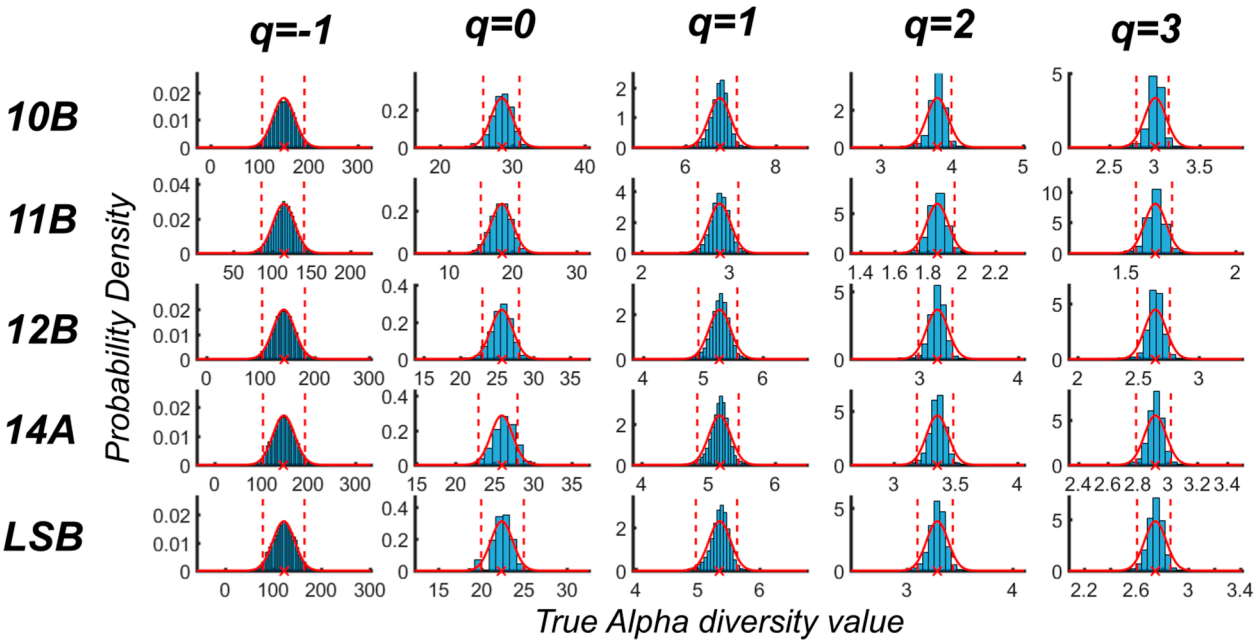

Figure S9. Resulting probability distributions in simulated true Alpha diversity metrics of orders -1,0,1,2,3 (column-wise) grouped by MC degrading community (row-wise) without the addition of ethanol. The solid red line indicates the normal probability distribution function fitted to the data, whereas the dashed red line indicates the 95% confidence interval for the distribution of each diversity order. The 'x' indicates the mean of each distribution.

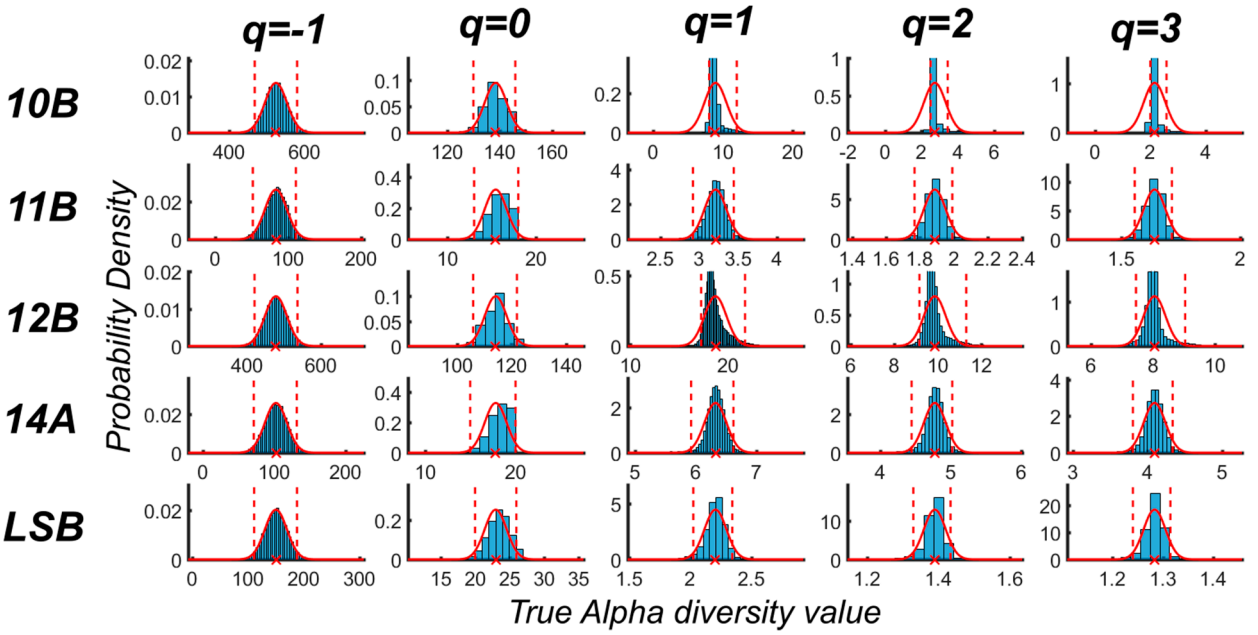

Figure S10 Resulting probability distributions in simulated true Alpha diversity metrics of orders -1,0,1,2,3 (column-wise) grouped by MC degrading community (row-wise) with the addition of ethanol. The solid red line indicates the normal probability distribution function fitted to the data, whereas the dashed red line indicates the 95% confidence interval for the distribution of each diversity order. The 'x' indicates the mean of each distribution.

Table S6 – Summary of normal distributions fitted to the MC simulation output in calculated Alpha diversity orders for consortia without ethanol addition.

Consortia ID	Metric	True Alpha diversity order				
		q = -1	q = 0	q = 1	q = 2	q = 3
10B	μ	149	28.6	6.76	3.79	3.01
	σ	22.1	1.50	0.241	0.152	0.119
	COV	14.8	5.2	3.6	4.0	4.0
11B	μ	115	18.3	2.89	1.85	1.64
	σ	13.9	1.70	0.125	0.0641	0.0493
	COV	12.1	9.3	4.3	3.5	3.0
12B	μ	143	25.7	5.28	3.18	2.64
	σ	20.1	1.49	0.182	0.110	0.0895
	COV	14.0	5.8	3.5	3.4	3.4
14A	μ	147	26.0	5.17	3.35	2.92
	σ	23.2	1.39	0.164	0.0872	0.0727
	COV	15.7	5.4	3.2	2.6	2.5
LSB	μ	122	22.4	5.36	3.29	2.75
	σ	22.6	1.28	0.175	0.102	0.0832
	COV	18.5	5.7	3.3	3.1	3.0

Table S7 – Summary of normal distributions fitted to the MC simulation output in calculated Alpha diversity orders for consortia with ethanol addition.

Consortia ID	Metric	True Alpha diversity order				
		q = -1	q = 0	q = 1	q = 2	q = 3
10B	μ	524	138	8.95	2.73	2.16
	σ	29.1	4.19	1.57	0.597	0.394
	COV	5.6	3.0	17.5	21.9	18.3
11B	μ	83.6	15.4	3.21	1.89	1.64
	σ	15.0	1.24	0.140	0.0644	0.0459
	COV	18.0	8.1	4.4	3.4	2.8
12B	μ	478	114	18.78	9.88	8.05
	σ	29.8	4.01	1.13	0.502	0.355
	COV	6.2	3.5	6.0	5.1	4.4
14A	μ	102	17.8	6.32	4.77	4.09
	σ	15.4	1.21	0.180	0.155	0.147
	COV	15.1	6.8	2.8	3.2	3.6
LSB	μ	150	23.0	2.21	1.39	1.28
	σ	19.7	1.59	0.0896	0.0307	0.0216
	COV	13.1	6.9	4.1	2.2	1.7

When comparing simulated diversity profiles of each MC-degrading community, with and without the addition of ethanol, there were distinct differences in trends across communities (Figure S11). For example, as diversity order increased, the dominance of certain genera (with higher relative abundance) increased for both the 10B and LSB communities (Figure S11). An opposing trend was observed for the 12B and 14A species, where the addition of ethanol may have an evening effect on the more abundant genera, as the slope of the diversity profile (with ethanol) is not as steep as compared to without (Figure S11). In addition, the differences in the diversity profiles for 11B consortium appear to be insignificant to make any definitive conclusions. These results confirm that ethanol addition had a unique effect on both the abundance and presence of certain genera within

each community, either increasing the evenness, increasing the dominance, or exerting a negligible effect as evidenced in Figure S11.

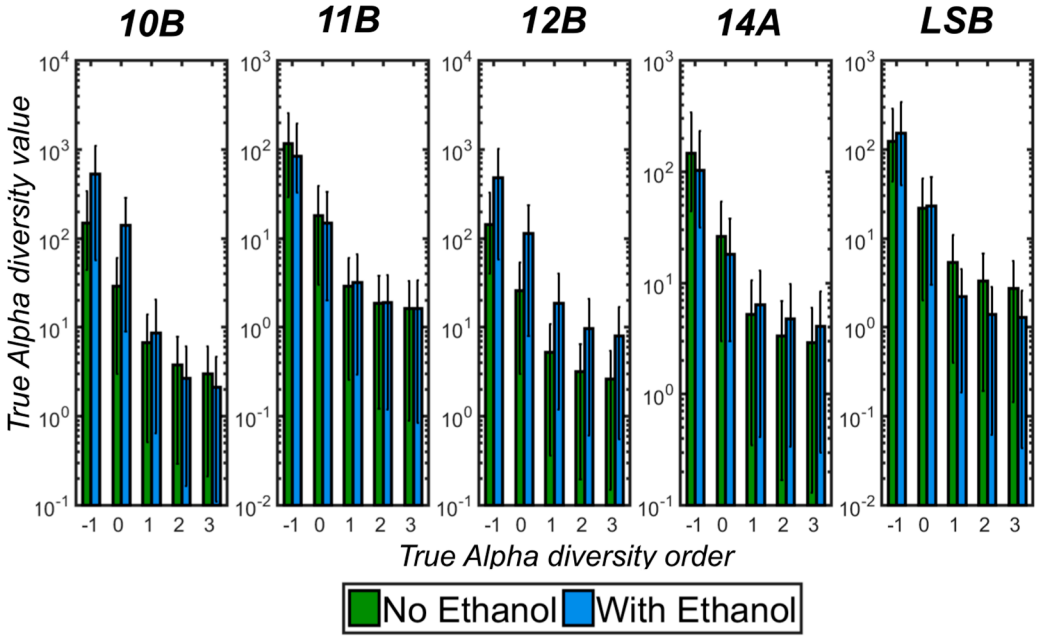

Figure S11 True Alpha diversity profiles for MC-degrading communities cultured with and without ethanol addition. The bar charts signify the median and 95% confidence intervals for the distributions of the true Alpha diversity values as a function of diversity order. The y-axis is plotted on a Log_{10}-scale to highlight the differences in diversity profiles between treatments.

We also present a summary of the "raw" Alpha diversity values as returned by the QIIME pipeline (Table S8). The "raw" indices include Shannon index, Simpson's Dominance, and Equitability values. These values were included as reference to existing studies that have reported similar "raw" indices for bacterial communities isolated from lakes of different trophic statuses.

Table S8 - Summary of "raw" Alpha diversity metrics for MC-LR degrading bacterial consortia without (NE) and with (WE) ethanol addition. Individual values of each metric are calculated for each of the five consortia within a given treatment.

Consortia ID	Culture Condition	Shannon Index	Simpson Dominance	Equitability
10B	NE	3.20	0.236	0.540
	WE	4.03	0.356	0.462
11B	NE	2.89	0.207	0.547
	WE	3.22	0.177	0.633
12B	NE	3.07	0.231	0.520
	WE	4.88	0.079	0.599
14A	NE	3.30	0.196	0.550
	WE	2.70	0.207	0.606
LSB	NE	3.82	0.104	0.666
	WE	3.18	0.208	0.545

(7) Quality Control of QIIME Analysis

A total of 66,716 16S rRNA gene reads were qualified for further QIIME metagenomics analysis from ten individual consortia samples after initial de-multiplexing, denoising, chimera removal and quality checking. The average number of 16S rRNA gene reads per sample was 6,672, ranging from

2,212 to 13,659 across all samples (Table S9). The average length of individual reads was approximately 488 base pairs, in which a majority of reads ranged between 300 to 500 base pairs in length (data not shown). A high percent recovery (OTU assignment/filtering retrieval) was observed for the Usearch quality filtering, clustering, and OTU picking. An average of 96% of the total reads were assigned to 690 distinct operational taxonomic units (Table S9).

Table S9- Summary of the consortia samples analyzed and the general results of the QIIME/Usearch analysis pipelines.

Consortia ID	Number of Reads Qualified	Number of Reads Retrieved	% Reads Retrieved
LR-NE-10B	6,790	6,527	96
LR-NE-11B	2,212	2,180	99
LR-NE-12B	5,758	5,390	94
LR-NE-14A	8,011	7,834	98
LR-NE-LSB	6,731	6,582	98
LR-WE-10B	13,659	12,384	91
LR-WE-11B	2,496	2,431	97
LR-WE-12B	12,380	11,364	92
LR-WE-14A	3,462	3,315	96
LR-WE-LSB	5,217	4,949	95
Total	66,716	62,956	96[1]

[1]This represents the average of the percentage of reads that were retrieved.

(8) Rarefaction Analysis

The Shannon indices as a function of the number of sequences retrieved by the QIIME module were investigated in the rarefaction analysis. It is evident that the sequencing depth was adequate for all consortia, as the Shannon indices were observed to plateau (Figure S12).

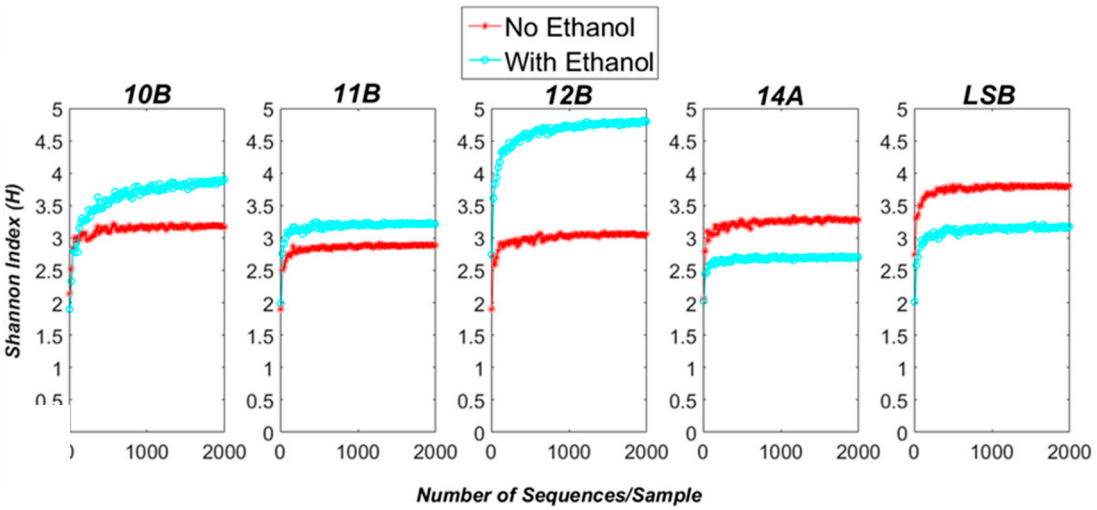

Figure S12 Rarefaction plots showing Shannon Diversity indices for microcystin-LR degrading consortia.

(9) Taxonomic Summary of MC-Degrading Communities on the Genera Level of Analysis

Figures S13-S15 further dissect the taxonomic composition of each MC-LR degrading community in the absence of ethanol on the genera level of analysis and are grouped by each representative order (i.e., *Rhizobiales*, *Burkholderiales*, *Xanthomonadales, or* "Other"). These orders were

selected for grouping each taxon since they represent a large proportion of taxa within each community. Figure S13, S14, and S15 depict the proportions of all detected genera within the *Rhizobiales Burkholderiales,* and *Xanthomonadales* orders. It is important to note that all of these genera were obtained by filtering out extremely underrepresented taxa from each consortium (relative abundance < 0.001 %).

As observed in each Figure below, there appears to be similar genera present (albeit in different proportions) within the sediment samples (10B-14A) as compared to the lake water sample (LSB). It is important to note that in Figure S16 the proportion of taxa on the genera level of analysis are portrayed from all remaining orders (i.e., the residuals not contained within *Rhizobiales Burkholderiales,* or *Xanthomonadales*). In addition, to better illustrate differences in composition, Figure S16 includes the taxonomic composition without the *Pseudomonas* (for 10B, 11B, 14A, LSB only) or *Azospirillum* (for 12B only) genera, as these taxa dominate the composition (>90%) of each community.

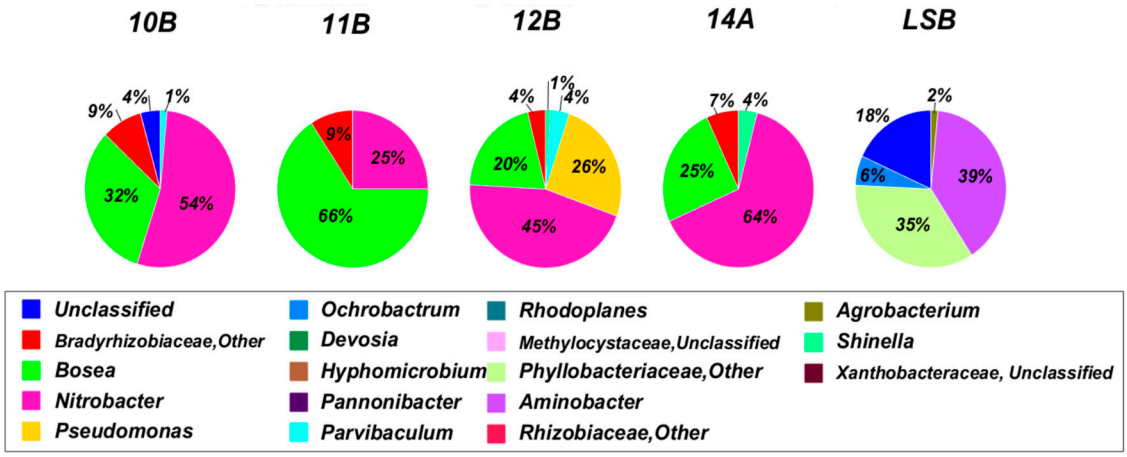

Figure S13 Pie charts depicting the taxonomic composition of MC-LR degrading communities (in the absence of ethanol) on the genera level of analysis within the *Rhizobiales* order.

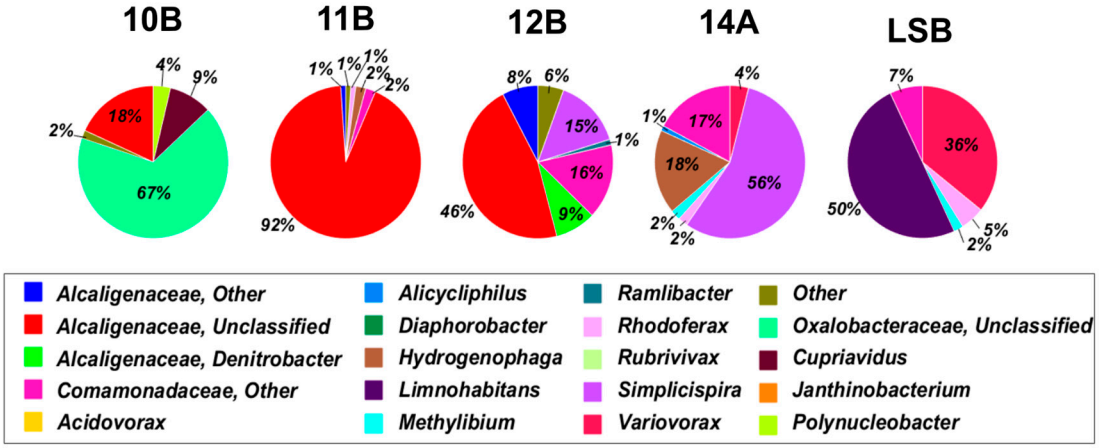

Figure S14 Pie charts depicting the taxonomic composition of MC-LR degrading communities (in the absence of ethanol) on the genera level of analysis within the *Burkholderiales* order.

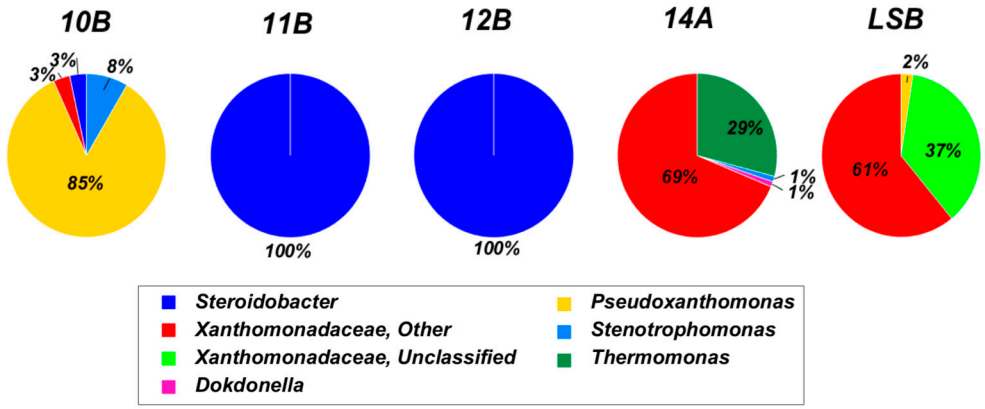

Figure S15 Pie charts depicting the taxonomic composition of MC-LR degrading communities (in the absence of ethanol) on the genera level of analysis within the *Xanthomonadales* order.

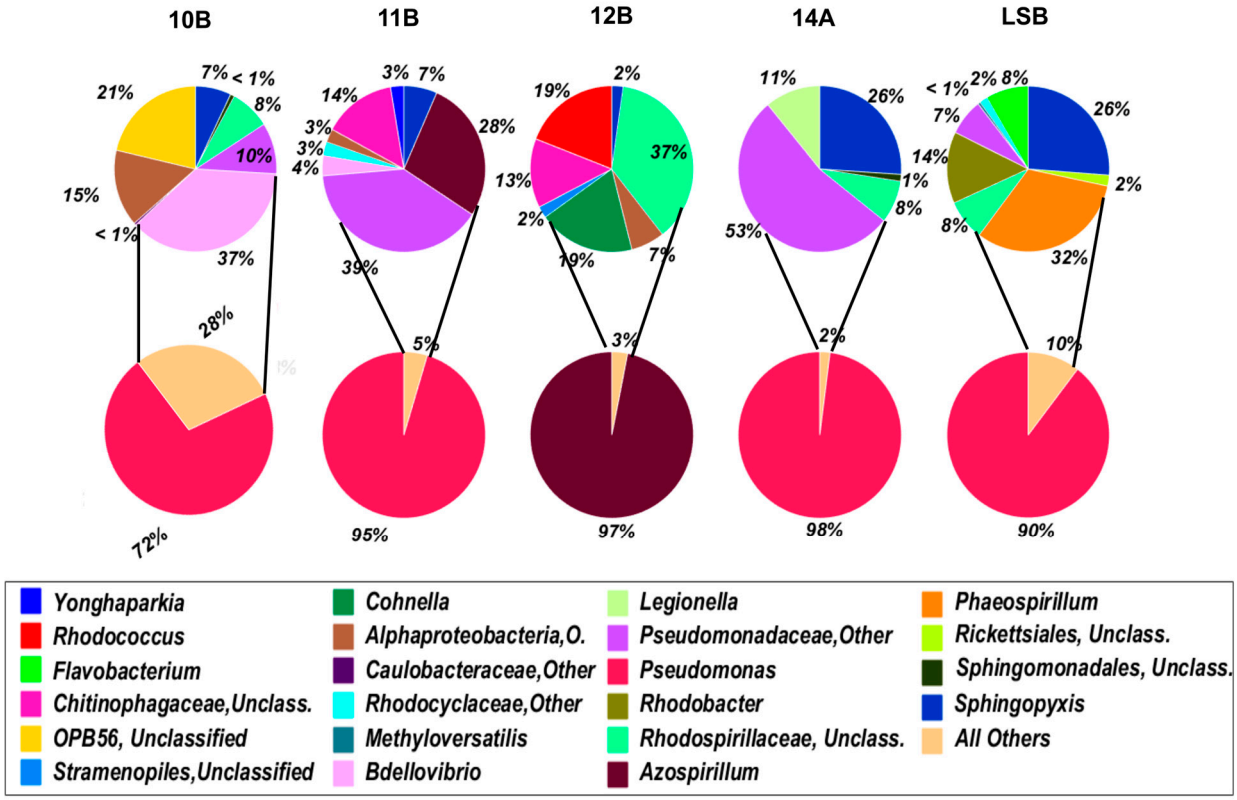

Figure S16 Pie charts depicting the taxonomic composition of MC-LR degrading communities (in the absence of ethanol) on the genera level of analysis within all remaining orders (other than *Rhizobiales*, *Burkholderiales*, or *Xanthomonadales*). It is important to note that the *Pseudomonas* genera (pictured here on the bottom row of pie charts) makes up 71.6, 95.3, 98, and 89% of the genera for the "Other" orders grouping for 10B,11B,14A, and LSB, respectively. In addition, the *Azospirillum* genera comprises 96.8% of the "Other" orders grouping for the 12B consortia. Thus, the pie charts on the top row above depict the proportions of the other genera without *Pseudomonas* (for 10B,11B,14A, and LSB only) or *Azosprillum* (for 12B only) included to highlight differences in the less representative taxa.

(10) Summary of Affiliated MC-Degrading Genera With and Without Ethanol Addition

Table S10 summarizes the bacterial genera present in different consortia that have been associated with species of MC-degrading bacteria. The bacterial genera identified within each consortium included the following: *Sphingopyxis*, *Sphingomonas*, *Acinetobacter*, *Aeromonas*,

Sphingomonas, *Novosphingobium*, *Pseudomonas*, *Stenotrophomonas*, *Ochrobactrum*, *Rhodococcus*, and *Steroidobacter*. Although 10 distinct genera were initially identified, not all genera were present in each consortium, as indicated in the "Consortia Detected" column. Several genera are affiliated with species that degrade MC using the well-known mlr gene pathway; however, several degrading pathways are either unknown or have not been detected (Table S10).

Table S10 – Bacterial genera identified within each consortium that have been previously affiliated with species of MC-degrading bacteria.

Bacterial Genera	Consortia Detected	*mlr* pathway?	Reference
Ochrobactrum	14A-NE, LSB-NE, 10B-WE, 14A-WE	Unknown	[41, 52]
Pseudomonas	10B-NE, 11B-NE, 14A-NE, LSB-NE, 10B-WE, 11B-WE, 14A-WE, LSB-WE	Unknown	[44, 98
Steroidobacter	10B-NE, 11B-NE, 12B-NE, LSB-NE, 10B-WE	Unknown	[102]
Stenotrophomonas	10B-NE, 14A-NE, 10B-WE, 12B-WE, 14A-WE	+	[31]
Sphingomonas	10B-NE, 14A-NE, 12B-NE	+	[28, 33, 38, 39, 51, 57, 62, 63]
Sphingopyxis	10B-NE, 11B-NE, 12B-NE,14A-NE, LSB-NE, 10B-WE, 12B-WE	+	[66-68, 100, 101]
Rhodococcus	12B-NE, 12B-WE	-	[26, 49]
Novosphingobium	12B-WE	+	[40]
Acinetobacter	10B-WE, 12B-WE	Unknown	[98]
Aeromonas	10B-WE, 12B-WE	-	[50]

Aside from the *Pseudomonas* genera, the relative abundance of the potential known MC degrading bacteria within each community was found to be relatively small and sometimes quite variable across each consortium (below 0.5-1%) With the addition of ethanol, the proportion of sequences from genera affiliated with MC biodegradation was observed to change significantly (Figure S17). In general, the relative abundance of bacterial species associated with the *Sphingopyxis* genera was observed to significantly decline across all consortia, whereas the relative abundance of bacterial species associated with the *Stenotrophomonas* was observed to significantly increase in the presence of ethanol (Figure S17). In addition, in the presence of ethanol, the relative abundance was observed to generally increase for the following bacterial genera: *Aeromonas*, *Acinetobacter*, *Novosphingobium*, and *Ochrobactrum* across all consortia. Some of these increases in relative abundance were not statistically significant (Figure S17). Trends in relative abundance were less apparent for the remaining genera affiliated with MC degradation across all consortia. For example, the relative abundance of *Steroidobacter* increased for 10B consortia in the presence of ethanol but decreased for 11B and 12B consortia. Similar mixed results were detected for the *Pseudomonas* genera with and without the addition of ethanol (Figure S17).

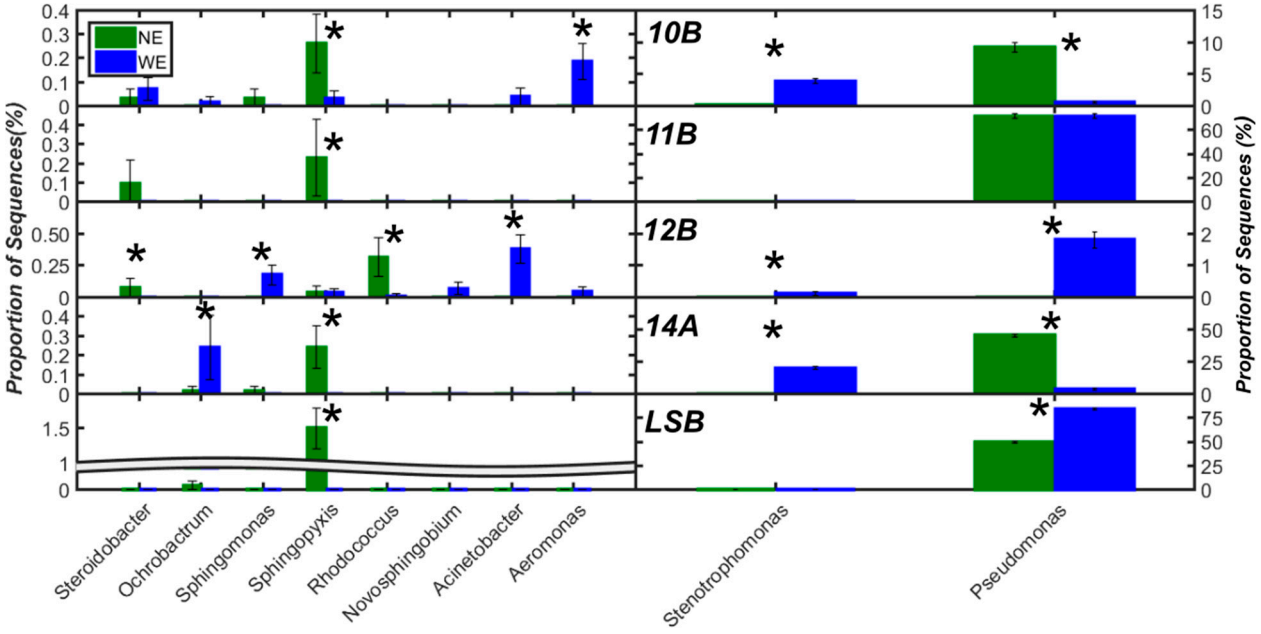

Figure S17 Differences in relative abundance of the phylogenetic genera previously affiliated with MC degradation that were identified within consortia treated with (WE) and without ethanol (NE). Statistically significant differences in relative abundance are marked with an asterisk (p-value < 0.05, Bonferroni corrected).

(11) Summary of Reported MC Biodegradation Half Lives

A detailed review of studies examining MC biodegradation kinetics was conducted to compare the half-lives for isolated MC degrading bacterial populations against those reported for enriched MC degrading consortia. The reported half-lives were estimated by each study using three unique approaches a) simply interpolating the time until 50% of the initial substrate was degraded [26]; b) fitting a zero-order model to the kinetic data [27] (Equations 13-14); or c) fitting a first-order model to the kinetic data [28] (Equations 15-16). If the study did not report a half-life value, we fitted a simple 0-order model to predict the MC biodegradation half-lives using the data provided in the study. A total of 50 [26, 28-76] and 27 [27, 28, 77–97] studies were compiled for MC degrading isolates and consortia, respectively. Only studies that focused on aerobic (not anaerobic) MC biodegradation through *bacterial* activity were incorporated in this analysis. All half-lives were included from each study for each experimental condition tested, regardless of environmental condition studied (i.e., pH, temperature, initial MC concentration), giving rise to a higher number of half-lives reported over studies compiled (i.e., N=167 vs. 27 studies). Comparably, we did not make a distinction between aqueous and biofilm MC degrading bacterial communities when compiling the reported half-lives for isolated consortia.

$$t_{1/2,0} = \frac{C_0}{2 * K_0} \quad (13)$$

where C_0 is the initial concentration of MC (μg/L) and K_0 is the zero-order rate constant (μg/L/day) determined using Eq. 2.

$$K_0 = \frac{(C_0 - C_F)}{\Delta t} \quad (14)$$

Where C_F is the final concentration of MC (μg/L, usually 0), and Δt is the total time elapsed until C_F is reached.

$$t_{1/2,1} = \frac{\ln(2)}{K_1} \quad (15)$$

Where K_1 (1/day) is the first order rate constant that is derived from fitting the experimental data to the first order kinetic equation. In the absence of non-linear curve fitting tools, K_1 can be estimated from Equation 4 using the natural logarithm of MC concentration.

$$K_1 = \frac{ln(C_0) - \ln(C_F)}{\Delta t} \quad (16)$$

where C_F is the final concentration of MC (μg/L, usually 0), and Δt is the total time elapsed until C_F is reached.

In general, isolated degrading populations demonstrated faster biodegradation kinetics than the enriched consortia studied (Figure S18). The statistical results of a two-tailed t-test with homoscedastic error variance (α = 0.05) indicated that the MC biodegradation half-lives for isolated degrading populations were significantly faster than those for enriched consortia (p = 2.45E-14). The distribution of reported biodegradation half-lives for isolated populations was also much narrower as compared to consortia (small interquartile range and whiskers), indicating that the biodegradation behavior was more consistent and less variable than isolated consortia. The range of half-lives predicted for consortia isolated in this study (without organic carbon) was within the 25-50% interquartile range for isolated consortia, signifying that the biodegradation kinetics were fast as compared to other kinetics reported in the literature for various consortia (Figure S18). However, the range of half-lives predicted for consortia isolated in this study (without organic carbon) was above the 50-75% interquartile range for isolated consortia, implying that the biodegradation kinetics for consortia may not be as rapid or comparable in efficiency to isolated degrading populations (Figure S18).

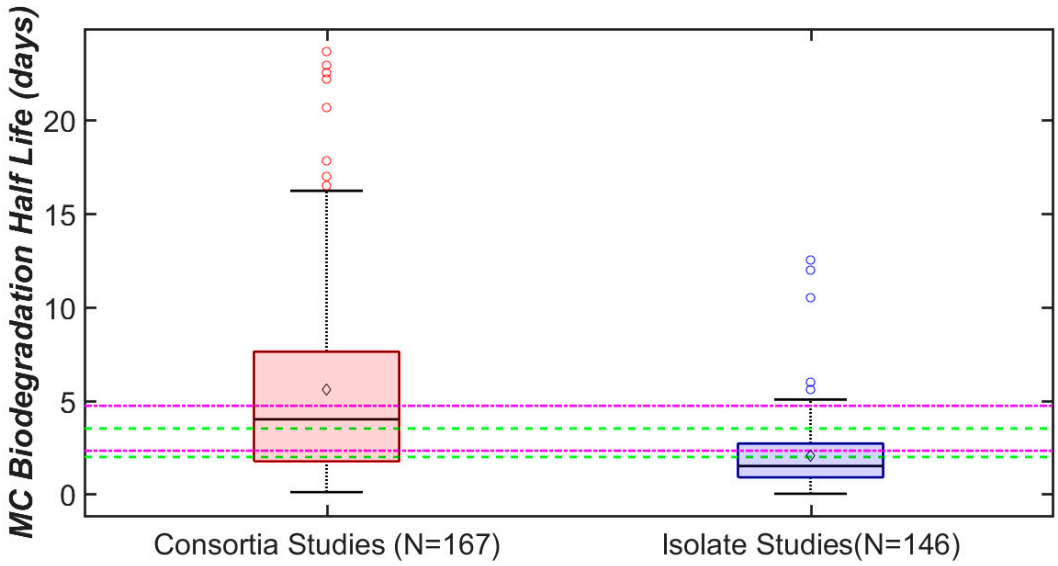

Figure S18 Boxplot summary of reported MC biodegradation half-lives in the literature for studies involving both enriched consortia and isolated degradation populations. The green and magenta dashed/dot-dashed lines indicate the range (average value ± 1 standard deviation) in predicted half-lives determined in this study for consortia without and with ethanol, respectively. The number of reported half lives used to develop each distribution is indicated in the x-axis title (i.e., N value). Black diamonds indicate mean biodegradation half-lives for each distribution.

(12) Monte Carlo Analysis to Assess the Effect of Sampling Frequency

In this section, we investigate to what extent the number of data points used in model calibration (which depends on the sampling frequency) will affect the main conclusions presented in the manuscript. This analysis was conducted out of our own mindfulness that the sampling frequency used in this study may not have been high enough to provide meaningful data. Ultimately, we argue that no matter how many data points are acquired during experimentation that may "fill the missing gaps" between existing data points (serving as "partials"), the main conclusions presented in the manuscript will not change significantly.

To prove our point, we have run a brief Monte Carlo (MCA) simulation using experimental results from the 11B consortium as an example. The 11B consortium was used since it demonstrated very similar MC-LR degradation kinetic profiles between the two treatments. We performed this MCA by simulating (or re-creating) our experimental dataset with a greater number of data points included (changing from N=7 to N=13) to represent the "what if" scenario of collecting more data points during experimentation. For example, using the original dataset as a foundation, three data points were simulated between Days 1 and 2 and three data points were simulated between Days 2 and 3, effectively doubling the number of datapoints in the dataset. Data points were added in the timeframe from Day 1 to Day 3 since this was the most dynamic portion of the experiment.

To run these MCA simulations, the simulated datapoints were taken as random, uniform draws using 0 and 200 (μg/L) as lower and upper boundaries of the selection interval. The selection of this interval for MCA sampling allows many different types of degradation behavior to be simulated during this time period. In addition, new selections were made from the existing data using normal, random draws (assuming the measurement error was normally distributed and using the mean and standard deviation obtained from the original measurements). Once the dataset was re-sampled, we performed non-linear, least squares regression to obtain a best-fitting parameter estimate and determined the half-lives from the best fitting prediction accordingly. This procedure was repeated for 50,000 unique simulations to arrive at a distribution in half-lives for statistical comparison between each treatment. Significant differences in predicted half-lives between both simulated datasets (between consortia with and without ethanol) were assessed using a two-sample t-test (two-sided, unequal variance). The effect size was also calculated to evaluate the magnitude of difference between both distributions (see Equation 4 in the manuscript).

The results of the MCA analysis indicated that the addition of new data points to the existing dataset did not change our initial conclusion presented in the manuscript, as MC-LR biodegradation half-lives between treatments remained significantly different (Table S11, under "MCA" tab). However, the standard deviations of the distribution in half-lives increased an order of magnitude with the introduction of new data points in the MCA analysis (Table S11). In addition, the values of the effect sizes presented for the original dataset were larger than those observed for the MCA modified datasets, suggesting that MCA simulation created more variability in the simulated MC-LR removal kinetics (i.e., with/without ethanol) (Table S11). This result provides enough quantitative evidence that even if we increased the sampling intensity between the time periods that demonstrated the most change, the main conclusions reached would not be drastically different.

Table S11 – Statistical comparison of simulated half-lives between treatments (with vs. without ethanol) for both original and MC analysis datasets.

Criteria	Original		MCA	
	11B-NE	**11B-WE**	**11B-NE**	**11B-WE**
μ	2.14	2.30	2.05	2.16
σ	0.017	0.016	0.314	0.293
p-value	<1E-08		<1E-08	
Effect Size	9.693		0.348	

Figure S19 visually demonstrates that the distribution in 50,000 simulated MC-LR degradation curves is relatively uniform (especially for panel B), despite the extremely wide range in concentrations sampled from (i.e., 0-200 μg/L) for each of the three time points between Days 1-2 or 2-3 of analysis. The relatively narrow 25-75% confidence interval bands indicate that although the concentrations of MC-LR in the simulated datasets were drastically changing, the model response was relatively similar across different MCA simulations. This result is because, mechanistically, the model cannot account for the very dynamic (perhaps up and down) degradation behavior simulated in the MCA analysis. Similar results were observed for the 12B and 14A consortia (without ethanol) in Figure 2 of the original manuscript, where the best fits of the model would pass through data points for Days 2 and 3 of analysis. Therefore, we can conclude (after assessing statistical and qualitative data) that even if we sampled more data points between Days 1-2 and 2-3, our initial conclusions would not change significantly. This result is due to the fact that the model is not sophisticated enough to mechanistically account for very dynamic changes in MC-LR concentrations over time.

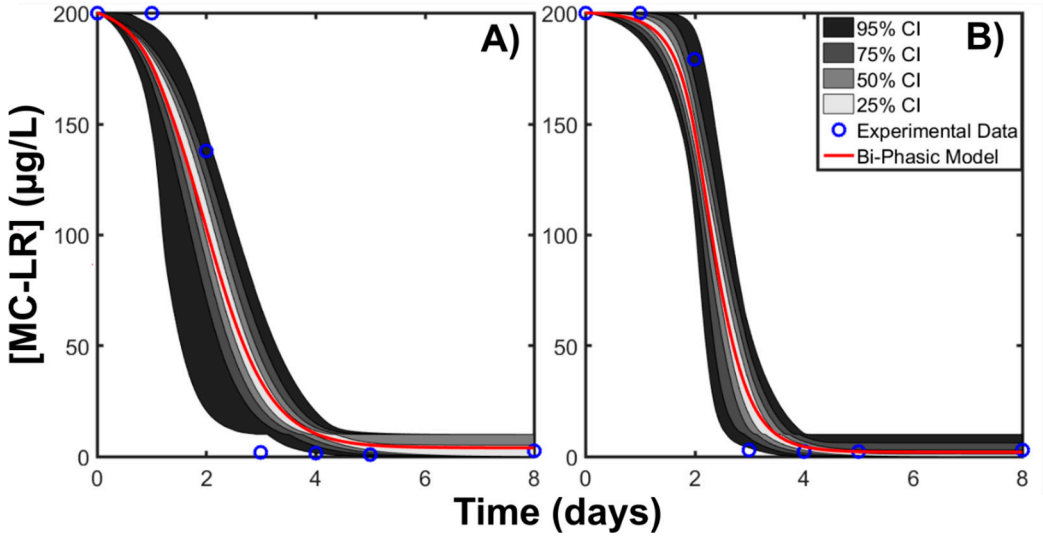

Figure S19. Distribution in simulated MC-LR biodegradation kinetics obtained from the MC analysis for consortia treated A) without ethanol and B) with ethanol. The shading indicates the nonparametric confidence intervals (25, 50, 75, and 95%) estimated from the distribution of kinetic curves obtained from the MC analysis. The blue circles represent the experimental data, whereas the red line indicates the mean of the 50,000 simulated MC-LR removal curves.

References

1. Huang, X.; Zhao, Z.; Hernandez, D.; Jiang, S.C. Near Real-Time Flow Cytometry Monitoring of Bacterial and Viral Removal Efficiencies during Water Reclamation Processes. *Water* **2016**, *8*, 464, doi:10.3390/w8100464.
2. Ouiroga, J.M.; Perales, J.A.; Romero, L.I.; Sales, D. Biodegradation kinetics of surfactants in seawater. *Chemosphere* **1999**, *39*, 1957–1969, doi:10.1016/S0045-6535(99)00077-6.
3. Vrugt, J.A. Markov chain Monte Carlo simulation using the DREAM software package: Theory, concepts, and MATLAB implementation. *Environ. Modell. Softw.* **2016**, *75*, 273–316, doi:10.1016/j.envsoft.2015.08.013.
4. Motulsky, H.; Christopoulos, A. *Fitting Models to Biological Data Using Linear and Nonlinear Regression: A Practical Guide to Curve Fitting*; Oxford University Press, 2004; ISBN 978-0-19-803834-4.
5. Rubin, DB; Gelman, A. Inference from Iterative Simulation Using Multiple Sequences. *Stat. Sci.* **1992**, 7, 457–472.
6. McLean, K.A.P.; McAuley, K.B. Mathematical modelling of chemical processes—obtaining the best model predictions and parameter estimates using identifiability and estimability procedures. *Can. J. Chem. Eng.* **2012**, *90*, 351–366, doi:10.1002/cjce.20660.

7. Holmberg, A. On the practical identifiability of microbial growth models incorporating Michaelis-Menten type nonlinearities. *Mathematical Biosciences* **1982**, *62*, 23–43, doi:10.1016/0025-5564(82)90061-X.
8. Nihtilä, M.; Virkkunen, J. Practical identifiability of growth and substrate consumption models. *Biotechnol. Bioeng.* **1977**, *19*, 1831–1850, doi:10.1002/bit.260191208.
9. Robinson, J.A.; Tiedje, J.M. Nonlinear estimation of Monod growth kinetic parameters from a single substrate depletion curve. *Appl. Environ. Microbiol.* **1983**, *45*, 1453–1458.
10. Liu, C.; Zachara, J.M. Uncertainties of Monod Kinetic Parameters Nonlinearly Estimated from Batch Experiments. *Environ. Sci. Technol.* **2001**, *35*, 133–141, doi:10.1021/es001261b.
11. Knight, R.; Jansson, J.; Field, D.; Fierer, N.; Desai, N.; Fuhrman, J.A.; Hugenholtz, P.; Lelie, D. van der; Meyer, F.; Stevens, R.; Bailey, M.J.; Gordon, J.I.; Kowalchuk, G.A.; Gilbert, J.A. Unlocking the potential of metagenomics through replicated experimental design. *Nature Biotechnology* **2012**, *30*, 513–520, doi:10.1038/nbt.2235.
12. Thomas, T.; Gilbert, J.; Meyer, F. Metagenomics - a guide from sampling to data analysis. *Microbial Informatics and Experimentation* **2012**, *2*, 3, doi:10.1186/2042-5783-2-3.
13. Chaudhary, A.; Kauser, I.; Ray, A.; Poretsky, R. Taxa-driven functional shifts associated with stormflow in an urban stream microbial community. *bioRxiv* **2018**, 300699, doi:10.1101/300699.
14. Landa, M.; Cottrell, M.T.; Kirchman, D.L.; Kaiser, K.; Medeiros, P.M.; Tremblay, L.; Batailler, N.; Caparros, J.; Catala, P.; Escoubeyrou, K.; Oriol, L.; Blain, S.; Obernosterer, I. Phylogenetic and structural response of heterotrophic bacteria to dissolved organic matter of different chemical composition in a continuous culture study. *Environmental Microbiology* **2014**, *16*, 1668–1681, doi:10.1111/1462-2920.12242.
15. Lopes, A.R.; Manaia, C.M.; Nunes, O.C. Bacterial community variations in an alfalfa-rice rotation system revealed by 16S rRNA gene 454-pyrosequencing. *FEMS Microbiol Ecol* **2014**, *87*, 650–663, doi:10.1111/1574-6941.12253.
16. Li, X.; Rui, J.; Mao, Y.; Yannarell, A.; Mackie, R. Dynamics of the bacterial community structure in the rhizosphere of a maize cultivar. *Soil Biology and Biochemistry* **2014**, *68*, 392–401, doi:10.1016/j.soilbio.2013.10.017.
17. Pereira, R.P.A.; Peplies, J.; Brettar, I.; Höfle, M.G. Development of a genus-specific next generation sequencing approach for sensitive and quantitative determination of the Legionella microbiome in freshwater systems. *BMC Microbiology* **2017**, *17*, 79, doi:10.1186/s12866-017-0987-5.
18. Pilloni, G.; Granitsiotis, M.S.; Engel, M.; Lueders, T. Testing the Limits of 454 Pyrotag Sequencing: Reproducibility, Quantitative Assessment and Comparison to T-RFLP Fingerprinting of Aquifer Microbes. *PLOS ONE* **2012**, *7*, e40467, doi:10.1371/journal.pone.0040467.
19. Sun, J.; Zhang, Q.; Zhou, J.; Wei, Q. Illumina Amplicon Sequencing of 16S rRNA Tag Reveals Bacterial Community Development in the Rhizosphere of Apple Nurseries at a Replant Disease Site and a New Planting Site. *PLOS ONE* **2014**, *9*, e111744, doi:10.1371/journal.pone.0111744.
20. Romanowicz, K.J.; Freedman, Z.B.; Upchurch, R.A.; Argiroff, W.A.; Zak, D.R. Active microorganisms in forest soils differ from the total community yet are shaped by the same environmental factors: the influence of pH and soil moisture. *FEMS Microbiol Ecol* **2016**, *92*, doi:10.1093/femsec/fiw149.
21. Huang, X.; Liu, L.; Wen, T.; Zhu, R.; Zhang, J.; Cai, Z. Illumina MiSeq investigations on the changes of microbial community in the *Fusarium oxysporum cubense* infected soil during and after reductive soil disinfestation. *Microbiological Research* **2015**, *181*, 33–42, doi:10.1016/j.micres.2015.08.004.
22. Zhou, X.; Wu, F. Vanillic acid changed cucumber (*Cucumis sativus L.*) seedling rhizosphere total bacterial, *Pseudomonas* and *Bacillus spp*. communities. *Scientific Reports* **2018**, *8*, 4929, doi:10.1038/s41598-018-23406-2.
23. Jacoby, W.G. Loess: a nonparametric, graphical tool for depicting relationships between variables. *Electoral Studies* **2000**, *19*, 577–613.
24. Efron, B.; Tibshirani, R.J. *An Introduction to the Bootstrap*; CRC Press, **1994**; ISBN 978-0-412-04231-7.
25. Gottschalk, F.; Scholz, R.W.; Nowack, B. Probabilistic material flow modeling for assessing the environmental exposure to compounds: Methodology and an application to engineered nano-TiO2 particles. *Environmental Modelling & Software* **2010**, *25*, 320–332, doi:10.1016/j.envsoft.2009.08.011.
26. Lawton, L.A.; Welgamage, A.; Manage, P.M.; Edwards, C. Novel bacterial strains for the removal of microcystins from drinking water. *Water Sci. Technol.* **2011**, *63*, 1137–1142, doi:10.2166/wst.2011.352.

27. Li, J.; Shimizu, K.; Akasako, H.; Lu, Z.; Akiyama, S.; Goto, M.; Utsumi, M.; Sugiura, N. Assessment of the factors contributing to the variations in microcystins biodegradability of the biofilms on a practical biological treatment facility. *Bioresour. Technol.* **2015**, *175*, 463–472, doi:10.1016/j.biortech.2014.10.047.
28. Jones, G.J.; Bourne, D.G.; Blakeley, R.L.; Doelle, H. Degradation of the cyanobacterial hepatotoxin microcystin by aquatic bacteria. *Nat. Toxins* **1994**, *2*, 228–235, doi:10.1002/nt.2620020412.
29. Alamri, S.A. Biodegradation of microcystin by a new *Bacillus sp.* isolated from a Saudi freshwater lake. *Afr. J Biotechnol.* **2010**, *9*, 6552–6559
30. Alamri, S.A. Biodegradation of microcystin-RR by *Bacillus flexus* isolated from a Saudi freshwater lake. *Saudi Journal of Biological Sciences* **2012**, *19*, 435–440, doi:10.1016/j.sjbs.2012.06.006.
31. Chen, J.; Hu, L.B.; Zhou, W.; Yan, S.H.; Yang, J.D.; Xue, Y.F.; Shi, Z.Q. Degradation of Microcystin-LR and RR by a *Stenotrophomonas sp.* Strain EMS Isolated from Lake Taihu, China. *International Journal of Molecular Sciences* **2010**, 11, 896–911, doi:10.3390/ijms11030896.
32. Eleuterio, L.; Batista, J.R. Biodegradation studies and sequencing of microcystin-LR degrading bacteria isolated from a drinking water biofilter and a fresh water lake. *Toxicon* **2010**, 55, 1434–1442, doi:10.1016/j.toxicon.2010.02.020.
33. Harada, K.; Imanishi, S.; Kato, H.; Mizuno, M.; Ito, E.; Tsuji, K. Isolation of Adda from microcystin-LR by microbial degradation. *Toxicon* **2004**, *44*, 107–109, doi:10.1016/j.toxicon.2004.04.003.
34. Ho, L.; Hoefel, D.; Saint, C.P.; Newcombe, G. Isolation and identification of a novel microcystin-degrading bacterium from a biological sand filter. *Water Research* **2007**, *41*, 4685–4695, doi:10.1016/j.watres.2007.06.057.
35. Ho, L.; Tang, T.; Monis, P.T.; Hoefel, D. Biodegradation of multiple cyanobacterial metabolites in drinking water supplies. *Chemosphere* **2012**, *87*, 1149–1154, doi:10.1016/j.chemosphere.2012.02.020.
36. Hu, L.B.; Yang, J.D.; Zhou, W.; Yin, Y.F.; Chen, J.; Shi, Z.Q. Isolation of a *Methylobacillus sp.* that degrades microcystin toxins associated with cyanobacteria. *New Biotechnology* **2009**, *26*, 205–211, doi:10.1016/j.nbt.2009.09.001.
37. Hu, L.; Zhang, F.; Liu, C.; Wang, M. Biodegradation of Microcystins by *Bacillus sp.* strain EMB. *Energy Procedia* **2012**, *16*, 2054–2059, doi:10.1016/j.egypro.2012.01.312.
38. Imanishi, S.; Kato, H.; Mizuno, M.; Tsuji, K.; Harada, K. Bacterial Degradation of Microcystins and Nodularin. *Chem. Res. Toxicol.* **2005**, *18*, 591–598, doi:10.1021/tx049677g.
39. Ishii, H.; Nishijima, M.; Abe, T. Characterization of degradation process of cyanobacterial hepatotoxins by a gram-negative aerobic bacterium. *Water Research* **2004**, *38*, 2667–2676, doi:10.1016/j.watres.2004.03.014.
40. Jiang, Y.; Shao, J.; Wu, X.; Xu, Y.; Li, R. Active and silent members in the mlr gene cluster of a microcystin-degrading bacterium isolated from Lake Taihu, China. *FEMS Microbiol. Lett.* **2011**, *322*, 108–114, doi:10.1111/j.1574-6968.2011.02337.x. (14)
41. Jing, W.; Sui, G.; Liu, S. Characteristics of a Microcystin-LR Biodegrading Bacterial Isolate: *Ochrobactrum sp.* FDT5. *Bull. Environ. Contam. Toxicol.* **2014**, *92*, 119–122, doi:10.1007/s00128-013-1170-9.
42. Kansole, M.M.R.; Lin, T.-F. Microcystin-LR Biodegradation by *Bacillus sp.*: Reaction Rates and Possible Genes Involved in the Degradation. *Water* **2016**, *8*, 508, doi:10.3390/w8110508.
43. Lemes, G.A.F.; Kersanach, R.; da S. Pinto, L.; Dellagostin, O.A.; Yunes, J.S.; Matthiensen, A. Biodegradation of microcystins by aquatic Burkholderia sp. from a South Brazilian coastal lagoon. *Ecotoxicology and Environmental Safety* **2008**, *69*, 358–365, doi:10.1016/j.ecoenv.2007.03.013.
44. Lemes, G.A.; Kist, L.W.; Bogo, M.R.; Yunes, J.S. Biodegradation of [D-Leu1] microcystin-LR by a bacterium isolated from sediment of Patos Lagoon estuary, Brazil. *J Venom Anim Toxins Incl Trop Dis* **2015**, 21, 4, doi:10.1186/s40409-015-0001-3.
45. Lezcano, M.Á.; Morón-López, J.; Agha, R.; López-Heras, I.; Nozal, L.; Quesada, A.; El-Shehawy, R. Presence or Absence of mlr Genes and Nutrient Concentrations Co-Determine the Microcystin Biodegradation Efficiency of a Natural Bacterial Community. *Toxins* **2016**, *8*, 318, doi:10.3390/toxins8110318.
46. Li, H.; Ai, H.; Kang, L.; Sun, X.; He, Q. Simultaneous *Microcystis* Algicidal and Microcystin Degrading Capability by a Single *Acinetobacter* Bacterial Strain. *Environ. Sci. Technol.* **2016**, *50*, 11903–11911, doi:10.1021/acs.est.6b03986.
47. Li, H.; Pan, G. Enhanced and continued degradation of microcystins using microorganisms obtained through natural media. *Journal of Microbiological Methods* **2014**, *96*, 73–80, doi:10.1016/j.mimet.2013.11.005.
48. Maghsoudi, E.; Fortin, N.; Greer, C.; Maynard, C.; Pagé, A.; Vo Duy, S.; Sauvé, S.; Prévost, M.; Dorner, S. Cyanotoxin degradation activity and mlr gene expression profiles of a *Sphingopyxis sp.* isolated from Lake

Champlain, Canada. *Environmental Science: Processes & Impacts* **2016**, *18*, 1417–1426, doi:10.1039/C6EM00001K.

49. Manage, P.M.; Edwards, C.; Singh, B.K.; Lawton, L.A. Isolation and Identification of Novel Microcystin-Degrading Bacteria. *Appl. Environ. Microbiol.* **2009**, *75*, 6924–6928, doi:10.1128/AEM.01928-09.
50. Mankiewicz-Boczek, J.; Gągała, I.; Jurczak, T.; Jaskulska, A.; Pawełczyk, J.; Dziadek, J. Bacteria homologus to *Aeromonas* capable of microcystin degradation. *Open Life Sciences* **2015**, *10*, doi:10.1515/biol-2015-0012.
51. Maruyama, T.; Park, H.-D.; Ozawa, K.; Tanaka, Y.; Sumino, T.; Hamana, K.; Hiraishi, A.; Kato, K. *Sphingosinicella microcystinivorans*, a microcystin-degrading bacterium. *Int J System Evol Microbiol* **2006**, *56*, 85–89, doi:10.1099/ijs.0.63789-0.
52. Mu, R.; He, Y.; Liu, S.; Wang, X.; Fan, Z. The Algicidal Characteristics of One Algae-Lysing FDT5 Bacterium on *Microcystis aeruginosa*. *Geomicrobiology Journal* **2009**, *26*, 516–521, doi:10.1080/01490450903061622.
53. Nybom, S.M.K.; Dziga, D.; Heikkilä, J.E.; Kull, T.P.J.; Salminen, S.J.; Meriluoto, J.A.O. Characterization of microcystin-LR removal process in the presence of probiotic bacteria. *Toxicon* **2012**, *59*, 171–181, doi:10.1016/j.toxicon.2011.11.008.
54. Nybom, S.M.K.; Collado, M.C.; Surono, I.S.; Salminen, S.J.; Meriluoto, J.A.O. Effect of Glucose in Removal of Microcystin-LR by Viable Commercial Probiotic Strains and Strains Isolated from Dadih Fermented Milk. *J. Agric. Food Chem.* **2008**, *56*, 3714–3720, doi:10.1021/jf071835x.
55. Nybom, S.M.K.; Salminen, S.J.; Meriluoto, J.A.O. Removal of microcystin-LR by strains of metabolically active probiotic bacteria. *FEMS Microbiol. Lett.* **2007**, *270*, 27–33, doi:10.1111/j.1574-6968.2007.00644.x.
56. Nybom, S.M.K.; Salminen, S.J.; Meriluoto, J.A.O. Specific strains of probiotic bacteria are efficient in removal of several different cyanobacterial toxins from solution. *Toxicon* **2008**, *52*, 214–220, doi:10.1016/j.toxicon.2008.04.169.
57. Park, H.-D.; Sasaki, Y.; Maruyama, T.; Yanagisawa, E.; Hiraishi, A.; Kato, K. Degradation of the cyanobacterial hepatotoxin microcystin by a new bacterium isolated from a hypertrophic lake. *Environ. Toxicol.* **2001**, *16*, 337–343, doi:10.1002/tox.1041.
58. Phujomjai, Y.; Somdee, A.; Somdee, T. Biodegradation of microcystin [Dha7]MC-LR by a novel microcystin-degrading bacterium in an internal airlift loop bioreactor. *Water Sci. Technol.* **2016**, *73*, 267–274, doi:10.2166/wst.2015.482.
59. Phujomjai, Y.; Somdee, T. Isolation and Characterization of Microcystin-Degrading Bacterium. *Journal of Life Sciences and Technologies* **2013**, *1*.
60. Ramani, A.; Rein, K.; Shetty, K.G.; Jayachandran, K. Microbial degradation of microcystin in Florida's freshwaters. *Biodegradation* **2012**, *23*, 35–45, doi:10.1007/s10532-011-9484-y.
61. Rapala, J.; Berg, K.A.; Lyra, C.; Niemi, R.M.; Manz, W.; Suomalainen, S.; Paulin, L.; Lahti, K. *Paucibacter toxinivorans*, a bacterium that degrades cyclic cyanobacterial hepatotoxins microcystins and nodularin. *International Journal of Systematic and Evolutionary Microbiology* **2005**, *55*, 1563–1568, doi:10.1099/ijs.0.63599-0.
62. Saitou, T.; Sugiura, N.; Itayama, T.; Inamori, Y.; Matsumura, M. Degradation characteristics of microcystins by isolated bacteria from Lake Kasumigaura. *J Water Supply: Res Technol* **2003**, *52*, 13–18.
63. Somdee, T. Biodegradation of cyanobacterial hepatotoxins [Dha^{7}]MC-LR and MC-LR by natural aquatic bacteria : a thesis submitted for fulfillment of the requirements for the degree of Doctor of Philosophy in Microbiology, Institute of Food, Nutrition and Human Health, College of Sciences, Massey University at Wellington, New Zealand, 2010.
64. Takenaka, S.; Watanabe, M.F. Microcystin LR degradation by *Pseudomonas aeruginosa* alkaline protease. *Chemosphere* **1997**, *34*, 749–757, doi:10.1016/S0045-6535(97)00002-7.
65. Valeria, A.M.; Ricardo, E.J.; Stephan, P.; Alberto, W.D. Degradation of Microcystin-RR by *Sphingomonas sp.* CBA4 isolated from San Roque reservoir (Córdoba – Argentina). *Biodegradation* **2006**, *17*, 447–455, doi:10.1007/s10532-005-9015-9.
66. Wang, J.; Wu, P.; Chen, J.; Yan, H. Biodegradation of Microcystin-RR by a New Isolated *Sphingopyxis sp.* USTB-05. *Chinese Journal of Chemical Engineering* **2010**, *18*, 108–112, doi:10.1016/S1004-9541(08)60330-4.
67. Xiao, C.; Yan, H.; Wang, J.; Wei, W.; Ning, J.; Pan, G. Microcystin-LR biodegradation by *Sphingopyxis sp.* USTB-05. *Front. Environ. Sci. Eng. China* **2011**, *5*, 526–532, doi:10.1007/s11783-010-0261-7.
68. Xu, H.; Wang, H.; Xu, Q.; Lv, L.; Yin, C.; Liu, X.; Du, H.; Yan, H. Pathway for Biodegrading Microcystin-YR by *Sphingopyxis sp.* USTB-05. *PLOS ONE* **2015**, *10*, e0124425, doi:10.1371/journal.pone.0124425.

69. Yang, F.; Zhou, Y.; Sun, R.; Wei, H.; Li, Y.; Yin, L.; Pu, Y. Biodegradation of microcystin-LR and-RR by a novel microcystin-degrading bacterium isolated from Lake Taihu. *Biodegradation* **2014**, *25*, 447–457, doi:10.1007/s10532-013-9673-y.
70. Yang, F.; Zhou, Y.; Yin, L.; Zhu, G.; Liang, G.; Pu, Y. Microcystin-Degrading Activity of an Indigenous Bacterial Strain *Stenotrophomonas acidaminiphila* MC-LTH2 Isolated from Lake Taihu. *PLOS ONE* **2014**, *9*, e86216, doi:10.1371/journal.pone.0086216.
71. You, D.J.; Chen, X.G.; Xiang, H.Y.; Ouyang, L.; Yang, B. Isolation, identification and characterization of a microcystin-degrading bacterium *Paucibacter sp.* strain CH. *Huan Jing Ke Xue* **2014**, *35*, 313–318.
72. Zhang, J.; Shi, H.; Liu, A.; Cao, Z.; Hao, J.; Gong, R. Identification of a New Microcystin-Degrading Bacterium Isolated from Lake Chaohu, China. *Bull Environ Contam Toxicol* **2015**, *94*, 661–666, doi:10.1007/s00128-015-1531-7.
73. Zhang, M.L.; Yan, H.; Pan, G. Microbial degradation of microcystin-LR by *Ralstonia solanacearum*. *Environmental Technology* **2011**, *32*, 1779–1787, doi:10.1080/09593330.2011.556148.
74. Zhou, J.; Yan, H.; He, H.; Zhong, G.; Lin, H.; Zhang, C. Activity of *Delftic acidovorans* for the Biodegradation of microcystins. *Science Technology & Engineering* **2006**, *2*.
75. Zhou, Y.; Yang, F.; Liang, G.; Yin, L.; Pu, Y. Biodegradation of Microcystin LR and RR by an indigenous bacterial strain MC-LTH11 isolated from Lake Taihu. *J Southeast University* **30**, 68–71
76. Zhu, X.; Shen, Y.; Chen, X.; Hu, Y.O.O.; Xiang, H.; Tao, J.; Ling, Y. Biodegradation mechanism of microcystin-LR by a novel isolate of *Rhizobium sp.* TH and the evolutionary origin of the mlrA gene. *Int. Biodeterioration Biodegrad.* **2016**, *115*, 17–25, doi:10.1016/j.ibiod.2016.07.011.
77. Bourne, D.G.; Blakeley, R.L.; Riddles, P.; Jones, G.J. Biodegradation of the cyanobacterial toxin microcystin LR in natural water and biologically active slow sand filters. *Water Research* **2006**, *40*, 1294–1302, doi:10.1016/j.watres.2006.01.022.
78. Chen, W.; Song, L.; Peng, L.; Wan, N.; Zhang, X.; Gan, N. Reduction in microcystin concentrations in large and shallow lakes: Water and sediment-interface contributions. *Water Research* **2008**, *42*, 763–773, doi:10.1016/j.watres.2007.08.007.
79. Christoffersen, K.; Lyck, S.; Winding, A. Microbial activity and bacterial community structure during degradation of microcystins. *Aquat. Microb. Ecol.* **2002**, *27*, 125–136, doi:10.3354/ame027125.
80. Cousins, I.T.; Bealing, D.J.; James, H.A.; Sutton, A. Biodegradation of microcystin-LR by indigenous mixed bacterial populations. *Water Research* **1996**, *30*, 481–485, doi:10.1016/0043-1354(95)00189-1.
81. Edwards, C.; Graham, D.; Fowler, N.; Lawton, L.A. Biodegradation of microcystins and nodularin in freshwaters. *Chemosphere* **2008**, 73, 1315–1321, doi:10.1016/j.chemosphere.2008.07.015.
82. Edwards, C.; Lawton, L.A. Bioremediation of Cyanotoxins. In *Adv. Appl. Microbiol.*; Laskin, A., Sariaslani, S., Gadd, G., Eds.; Academic Press, 2009; Vol. 67, pp. 109–129.
83. Grützmacher, G.; Wessel, G.; Klitzke, S.; Chorus, I. Microcystin Elimination During Sediment Contact. *Environ. Sci. Technol.* **2010**, 44, 657–662, doi:10.1021/es9016816.
84. Ho, L.; Hoefel, D.; Palazot, S.; Sawade, E.; Newcombe, G.; Saint, C.P.; Brookes, J.D. Investigations into the biodegradation of microcystin-LR in wastewaters. *J Hazard. Mater.* **2010**, *180*, 628–633, doi:10.1016/j.jhazmat.2010.04.081.
85. Ho, L.; Meyn, T.; Keegan, A.; Hoefel, D.; Brookes, J.; Saint, C.P.; Newcombe, G. Bacterial degradation of microcystin toxins within a biologically active sand filter. *Water Research* **2006**, *40*, 768–774, doi:10.1016/j.watres.2005.12.009.
86. Hoefel, D.; Adriansen, C.M.M.; Bouyssou, M.A.C.; Saint, C.P.; Newcombe, G.; Ho, L. Development of an mlrA Gene-Directed TaqMan PCR Assay for Quantitative Assessment of Microcystin-Degrading Bacteria within Water Treatment Plant Sand Filter Biofilms. *Appl. Environ. Microbiol.* **2009**, *75*, 5167–5169, doi:10.1128/AEM.00036-09.
87. Hyenstrand, P.; Rohrlack, T.; Beattie, K.A.; Metcalf, J.S.; Codd, G.A.; Christoffersen, K. Laboratory studies of dissolved radiolabelled microcystin-LR in lake water. *Water Research* **2003**, *37*, 3299–3306, doi:10.1016/S0043-1354(03)00180-5.
88. Jones, G.J.; Orr, P.T. Release and degradation of microcystin following algicide treatment of a Microcystis aeruginosa bloom in a recreational lake, as determined by HPLC and protein phosphatase inhibition assay. *Water Research* **1994**, *28*, 871–876, doi:10.1016/0043-1354(94)90093-0.

89. Lam, A.K.-Y.; Fedorak, P.M.; Prepas, E.E. Biotransformation of th cyanobacterial hepatotoxin microcystin-LR, as determined by HPLC and protein phosphatase bioassay. *Environ. Sci. Technol.* **1995**, 29, 242–246.
90. Lam, A.K.-Y.; Prepas, E.E.; Spink, D.; Hrudey, S.E. Chemical control of hepatotoxic phytoplankton blooms: Implications for human health. *Water Research* **1995**, *29*, 1845–1854, doi:10.1016/0043-1354(94)00348-B.
91. Li, J.; Shimizu, K.; Maseda, H.; Lu, Z.; Utsumi, M.; Zhang, Z.; Sugiura, N. Investigations into the biodegradation of microcystin-LR mediated by the biofilm in wintertime from a biological treatment facility in a drinking-water treatment plant. *Bioresour. Technol.* **2012**, *106*, 27–35, doi:10.1016/j.biortech.2011.11.099.
92. Li, J.; Shimizu, K.; Sakharkar, M.K.; Utsumi, M.; Zhang, Z.; Sugiura, N. Comparative study for the effects of variable nutrient conditions on the biodegradation of microcystin-LR and concurrent dynamics in microcystin-degrading gene abundance. *Bioresour. Technol.* **2011**, *102*, 9509–9517, doi:10.1016/j.biortech.2011.07.112.
93. Li J, Shimizu K, Utsumi M, et al (2011b) Dynamics of the functional gene copy number and overall bacterial community during microcystin-LR degradation by a biological treatment facility in a drinking water treatment plant. J Biosci Bioeng 111:695–701. doi: 10.1016/j.jbiosc.2011.02.007
94. Rapala, J.; Lahti, K.; Sivonen, K.; Niemelä, S.I. Biodegradability and adsorption on lake sediments of cyanobacterial hepatotoxins and anatoxin-a. *Letters in Applied Microbiology* **1994**, *19*, 423–428, doi:10.1111/j.1472-765X.1994.tb00972.x.
95. Tsao, S.; Wei, D.-J.; Chang, Y.-T.; Lee, J.-F. Aerobic biodegradation of microcystin-LR by an indigenous bacterial mixed culture isolated in Taiwan. *Int. Biodeterioration Biodegrad.* **2017**, doi:10.1016/j.ibiod.2017.04.011.
96. Wang, X.; Utsumi, M.; Gao, Y.; Li, Q.; Tian, X.; Shimizu, K.; Sugiura, N. Influences of metal ions on microcystin-LR degradation capacity and dynamics in microbial distribution of biofilm collected from water treatment plant nearby Kasumigaura Lake. *Chemosphere* **2016**, *147*, 230–238, doi:10.1016/j.chemosphere.2015.12.067.
97. Welker, M.; Steinberg, C.; Jones, G.J. Release and Persistence of Microcystins in Natural Waters. In *Cyanotoxins: Occurence, Causes, Consequences*; Springer Berlin Heidelberg, 2001; pp. 83–102.
98. Li, H.; Pan, G. Enhanced and continued degradation of microcystins using microorganisms obtained through natural media. *Journal of Microbiological Methods* **2014**, 96, 73–80, doi:10.1016/j.mimet.2013.11.005.
99. Li, H.; Ai, H.; Kang, L.; Sun, X.; He, Q. Simultaneous Microcystis Algicidal and Microcystin Degrading Capability by a Single Acinetobacter Bacterial Strain. *Environ. Sci. Technol.* **2016**, 50, 11903–11911, doi:10.1021/acs.est.6b03986.
100. Okano, K.; Shimizu, K.; Kawauchi, Y.; Maseda, H.; Utsumi, M.; Zhang, Z.; Neilan, B.A.; Sugiura, N. Characteristics of a Microcystin-Degrading Bacterium under Alkaline Environmental Conditions. *J Toxicol* **2009**, 2009, doi:10.1155/2009/954291.
101. Maghsoudi, E.; Fortin, N.; Greer, C.; Maynard, C.; Pagé, A.; Vo Duy, S.; Sauvé, S.; Prévost, M.; Dorner, S. Cyanotoxin degradation activity and mlr gene expression profiles of a Sphingopyxis sp. isolated from Lake Champlain, Canada. *Environmental Science: Processes & Impacts* **2016**, 18, 1417–1426, doi:10.1039/C6EM00001K.
102. Gong, Z.-L.; Zhang, C.-F.; Jin, R.; Zhang, Y.-Q. *Steroidobacter*, a microcystin-degrading Gammaproteobacterium isolated from soil. *Antonie van Leeuwenhoek* **2016**, 109, 1073–1079, doi:10.1007/s10482-016-0706-5.